

The global atmospheric electric circuit and its effects on cloud microphysics

B A Tinsley

Physics Department and Center for Space Sciences, WT15, University of Texas at Dallas,
800 W Campbell Road, Richardson, TX, 75080-3021, USA

E-mail: Tinsley@UTDallas.edu

Received 4 May 2007, in final form 13 February 2008

Published 2 May 2008

Online at stacks.iop.org/RoPP/71/066801

Abstract

This review is an overview of progress in understanding the theory and observation of the global atmospheric electric circuit, with the focus on its dc aspects, and its short and long term variability. The effects of the downward ionosphere-earth current density, J_z , on cloud microphysics, with its variability as an explanation for small observed changes in weather and climate, will also be reviewed. The global circuit shows responses to external as well as internal forcing. External forcing arises from changes in the distribution of conductivity due to changes in the cosmic ray flux and other energetic space particle fluxes, and at high magnetic latitudes from solar wind electric fields. Internal forcing arises from changes in the generators and changes in volcanic and anthropogenic aerosols in the troposphere and stratosphere. All these result in spatial and temporal variation in J_z .

Variations in J_z affect the production of space charge in layer clouds, with the charges being transferred to droplets and aerosol particles. New observations and new analyses are consistent with non-negligible effects of the charges on the microphysics of such clouds. Observed effects are small, but of high statistical significance for cloud cover and precipitation changes, with resulting atmospheric temperature, pressure and dynamics changes. These effects are detectable on the day-to-day timescale for repeated J_z changes of order 10%, and are thus second order electrical effects. The implicit first order effects have not, as yet, been incorporated into basic cloud and aerosol physics. Long term (multidecadal through millennial) global circuit changes, due to solar activity modulating the galactic cosmic ray flux, are an order of magnitude greater at high latitudes and in the stratosphere, as can be inferred from geological cosmogenic isotope records. Proxies for climate change in the same stratified depositories show strong correlations of climate with the inferred global circuit variations.

The theory for electrical effects on scavenging of aerosols in clouds is reviewed, with several microphysical processes having consequences for contact ice nucleation; effects on droplet size distributions; precipitation and cloud lifetimes. There are several pathways for resulting macroscopic cloud changes that affect atmospheric circulation; including enhanced ice production and precipitation from clouds in cyclonic storms, with latent heat release affecting cyclone vorticity; and cloud cover changes in layer clouds that affect the atmospheric radiation balance. These macroscopic consequences of global circuit variability affecting aerosols–cloud interactions provide explanations for the many observations of short term and long term changes in clouds and climate that correlate with measured or inferred J_z and cosmic ray flux changes due to external or internal forcing, and lead to predictions of additional effects.

This article was invited by Professor A Kostinski.

Contents

1. Historical perspective and introduction	2	5. Observed cloud and meteorological responses to inferred V_i and J_z changes	17
2. Global circuit fundamentals	3	5.1. <i>Observations of charges on droplets at cloud boundaries</i>	17
2.1. <i>General properties of the circuit</i>	3	5.2. <i>Macroscopic cloud and meteorological responses</i>	18
2.2. <i>Ion-pair production</i>	5	6. Theory for electrical effects of charge on scavenging	21
2.3. <i>Mobility of ions and local electric field</i>	7	6.1. <i>Calculating the electrical force</i>	21
2.4. <i>Ion loss processes</i>	8	6.2. <i>Calculating the trajectories and collision efficiencies</i>	23
2.5. <i>Production of space charge</i>	10	6.3. <i>Calculating the scavenging rates</i>	24
3. Modeling the dc properties of the global circuit	12	7. Summary and needs for further work	25
3.1. <i>Results of a global circuit model</i>	12	7.1. <i>Progress to date</i>	25
3.2. <i>Modifications and additions to models</i>	13	7.2. <i>Needed further work</i>	25
4. Global circuit time variations from internal and external inputs	14	Acknowledgments	26
4.1. <i>Diurnal through solar cycle variations</i>	14	References	27
4.2. <i>Long term variations</i>	16		

1. Historical perspective and introduction

The study of atmospheric electricity is one of the oldest geophysical sciences, and the work of Benjamin Franklin did much to advance this field and bring it to popular attention (e.g. Franklin 1752). The history of the field has been reviewed in books by Chalmers (1949/1967) and Israël (1957/1970, 1961/1973). Aspects of atmospheric electricity have been reviewed by Stow (1969), Mühleisen (1977), US National Academy of Sciences (NAS 1986), Reiter (1992), Bering *et al* (1988), Rycroft and Cho (1998), Rakov and Uman (2003), Harrison (2004a), Williams (2005), Rycroft (2006), Siingh *et al* (2007) and Markson (2007).

Early studies of atmospheric electricity were largely focused on the occurrence of lightning and the means for protecting buildings from damage due to lightning strokes, although the occurrence of the vertical atmospheric electric field, of order 100 V m^{-1} in fair weather, was well known. In the early 20th century the search for a mechanism to explain fair weather electricity led Wilson (1920) to the concept of the global electric circuit, in which the ionosphere served as a highly conducting layer in which upward current generated by thunderstorms was distributed over the whole globe, with the return current appearing as a downward current density distributed through the whole of the weakly conducting atmosphere, thus generating the observed electric fields near the surface. The atmospheric conductivity is due mainly to ionization by the variable galactic cosmic ray (GCR) flux, and conduction currents are carried by positive air ions moving in the direction of the electric field, and negative air ions moving in the opposite direction. (Electrons resulting from GCR ionization of air molecules are attached to other air molecules in microseconds.) The circuit is completed through the highly conducting (land and sea) Earth's surface, and vertical currents and negative cloud-to-ground lightning between the surface and the base of the cloud generators. The circuit can be compared with a leaky capacitor with plates consisting of a pair of concentric spherical shells.

The ionosphere is charged to a potential, V_i , relative to the Earth's surface, that is usually in the range 200–300 kV, by positive charge flowing upward as a conduction current, in the order of 1 A per storm from about 1000 thunderstorms and other highly electrified storm clouds, including shower clouds, around the globe (Williams 2005). The total current output, I_T , of these has temporal variations due to changes in the diurnal solar heating in the regions of deep convection and thunderstorms, modulated by the distribution of land masses around the tropics. The global sum of these local time variations produces a universal time variation in I_T , which has an amplitude of about $\pm 20\%$, for which an average variation was obtained in terms of near-surface electric fields by Torreson *et al* (1946) and is known as the 'Carnegie curve'.

It was shown by Whipple (1929) that the shape of this curve is similar to that of the variation of worldwide thunderstorm activity. However, while thunderstorm and lightning frequencies have been used as proxies for the charging of the ionosphere, intracloud lightning and positive cloud-to-ground lightning often serve to discharge the generators, which otherwise might produce a greater output of dc current to the ionosphere. Also, some clouds producing lightning have opposite polarity and discharge the ionosphere.

MacGorman and Rust (1998) have provided a comprehensive review of the understanding, up to the late 20th century, of the electrification of thunderstorms, and Rakov and Uman (2003) have provided a similar review for lightning. Recent papers by Stolzenburg *et al* (2002) and Davydenko *et al* (2004) have discussed how the complex and variable structure and charge distribution in clouds leads to a variable contribution to the current flow in the global circuit. Most deep convective clouds (not necessarily at thunderstorm stage) charge the ionosphere by mechanical separation of charge, carried by ice particles. The small ice particles are carried up by updrafts, usually being positively charged after collision with larger ice particles, including graupel, which are left negatively charged. The larger ice particles carry the negative charge down by means of their larger fall speeds. From cloud tops that are usually at

potentials much greater than the 250 kV of the ionosphere, conduction current flows upwards, through air of rapidly increasing conductivity, to maintain the global ionospheric potential and sustain the global return current.

Below the clouds, negative cloud to surface lightning, conduction and point discharge current and negatively charged rainfall (Soula *et al* 2003) all increase cloud potential and maintain the upward flow of current to the ionosphere. Above the clouds, transient discharges to the ionosphere, as detected in transient luminous events (Sentman and Wescott 1995, Lyons 1996, Pasco *et al* 1998) may affect the output of the electrified clouds.

Quantitative models of the variation of I_T with surface heating and aerosol concentrations and the GCR flux are not yet available. There is also a need to model the variations with climate oscillations at low latitude (e.g. the El Niño oscillation), and with longer term atmospheric climate changes. A discussion of estimates of the relatively large changes in I_t which are possible on multidecadal and longer time scales are given in section 4.2, but we do not attempt to review the physics of thunderstorms and lightning, nor the phenomena of transient discharges to the ionosphere.

Models of the dc aspects of the global circuit have been made by Hays and Roble (1979), Roble and Hays (1979), Makino and Ogawa (1985), Tzur *et al* (1983), Roble and Tzur (1986) and Sapkota and Varshneya (1990). These have varying degrees of completeness. In a recent model by Tinsley and Zhou (2006), which included a detailed treatment of tropospheric and stratospheric aerosols, the resistance, R_T , of the whole atmosphere, acting as a load between the concentric spherical conductors of the ionosphere and the surface, was calculated to vary between about 200 and 250 Ω , subject to variations due to the changing GCR flux, and variations due to changing natural and anthropogenic aerosols concentrations.

In this review we will focus on the global distribution of the spatial and temporal variability of the ionosphere-earth current density J_z , and the forcing of it by solar activity and the internal variability of the circuit. The variability of J_z depends partly on variations in atmospheric conductivity, due to variations in the external and internal sources of atmospheric ionization and of aerosols, and partly on V_i , which is mainly determined by the output of the internal generator comprising highly electrified clouds, but also by solar wind electric fields penetrating into the ionospheres of the magnetic polar cap regions.

We will also pay particular attention of the effects of J_z and its variability on layer clouds and other non-generator clouds that are present through most of the troposphere. Because the resistivity, r (inverse conductivity) of cloudy air is much greater than that of clear air at the same altitude (by a factor of between 3 and 30 according to Griffiths *et al* (1974) and Pruppacher and Klett (1997)) the flow of J_z through gradients of r at cloud boundaries produces a gradient in electric field E at that location. In addition, gradients in r and E are produced by fluctuations in droplet concentration in clouds and by layered structure and fluctuations in aerosol concentration outside clouds, due to convection and turbulence. These gradients in E must be accompanied by the presence of space charge ρ according to Gauss's Law, where $\rho = \epsilon_0 \nabla \cdot E$. The

response of space charge to the resistivity changes and to J , where $E = Jr$ is thus $\rho = \epsilon_0 J \nabla \cdot r$, assuming quasi-steady state conditions and constant J .

The space charge arises as the separation of positive and negative air ions, but these rapidly attach to droplets and aerosol particles including cloud condensation nuclei (CCN) and ice-forming nuclei (IFN). The electric charges on these particles affect the rate at which they are scavenged by droplets or by larger particles (Pruppacher and Klett 1997, section 18.6, Tinsley *et al* 2000, Tripathi and Harrison 2002, Harrison and Carslaw 2003) and the consequent macroscopic effects on clouds provides an explanation for many observations of cloud cover and related meteorological changes, which, in the absence of GCR flux changes, correlate with solar activity and J_z . These correlations are discussed in section 5.2. In the presence of GCR flux changes, the ion concentration that determines the conductivity in the global circuit varies with the GCR flux, and there are numerous reports, also discussed in section 5.2, of cloud cover and related meteorological changes that correlate with the GCR flux. A listing of these effects and references to papers showing the correlations is given in appendix A, and a list of acronyms is given in appendix B.

Ion-induced nucleation of aerosol particles (Dickinson 1975, Yu and Turco 2001, Harrison and Carslaw 2003, Kazil and Lovejoy 2004) that may grow to become CCN has been considered to provide an explanation for the correlations with the GCR flux, which is an alternative to that of effects due to J_z variations that accompany the GCR variations when they occur. The review of observations and possible mechanisms will lead to the conclusion that the ionization of the atmosphere, and the current that flows through it forming the global atmospheric electric circuit, act as agents contributing to weather and climate change.

2. Global circuit fundamentals

2.1. General properties of the circuit

2.1.1. Geometry of the global circuit. Figure 1 is a schematic circuit diagram of a part of the global circuit, as a section through the dawn–dusk magnetic meridian. The diagram represents the land and ocean surface as one spherical highly conducting circuit element, and above that the ionosphere forms a concentric outer conducting shell. The ionosphere above 90 km is where the external generators are active. This is in contrast to the concept of an effective upper boundary in the stratosphere which acts as a shield and has been called the ‘electrosphere’ (Chalmers 1949/1967). The conductivity of the stratosphere and mesosphere is usually, but not always, very high compared with that of the troposphere, so that the potential of the stratosphere at about 30 km has been described as being at 99% of ionospheric potential Markson (1971). As discussed in section 3.2.3, there are theoretical and observational grounds for layers of higher resistivity in the stratosphere at mid-high latitudes in the absence of relativistic electron precipitation, that are highly enhanced following volcanic eruptions. The Wilson (1920) upper boundary was the ionosphere, however we can consider the upper boundary as being as low as 60 km,

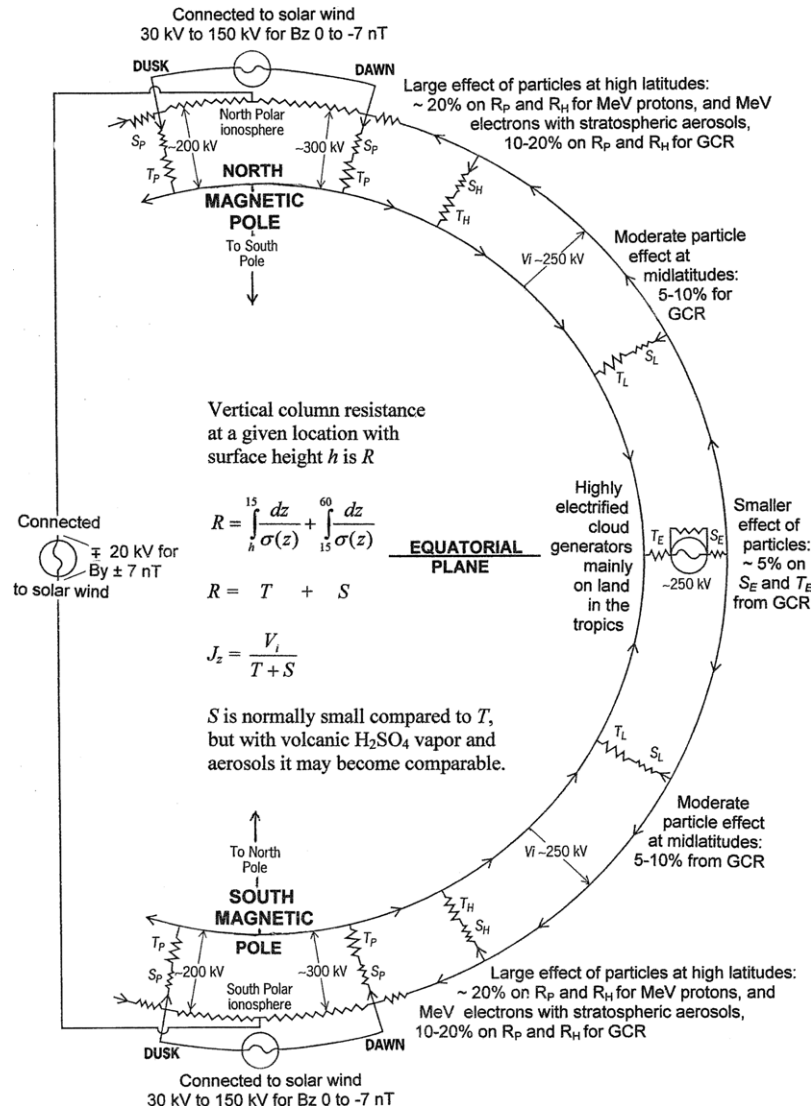


Figure 1. Schematic of a section through the global atmospheric electric circuit in the dawn–dusk magnetic meridian. The tropospheric and stratospheric column resistances at a given location are represented by T and S , with subscripts referring to equatorial, low, middle, high, and polar latitudes. The geometry is essentially plane-parallel, with only small changes in T due to changes in cosmic ray fluxes at low latitudes, but large changes in T and S due to cosmic ray and other energetic space particle fluxes at high latitudes. The variable solar wind generators affect V_i at high latitudes, and the variable highly electrified cloud generators, represented by the generator symbol in the equatorial plane, affect V_i globally, and volcanic aerosols as well as the energetic particles affect T and S ; with all acting together to modulate the ionosphere–earth current density J_z .

while still including in the circuit the high resistivity layers in the stratosphere.

In figure 1 thunderstorms and other highly electrified clouds that act as the internal (Wilsonian) generators for the global circuit are represented by the generator symbol at the equator.

The resistance, R , of a column of unit cross section between the ionosphere and the surface (land and sea) at any location is the vertical integral of the resistivity r , which is the reciprocal of the conductivity, σ . The values of R and V_i determine J_z for that location by Ohm’s Law, $J_z = V_i/R$. As indicated in figure 1, $R = \int_h^{60} dz/\sigma(z)$, with h being the altitude of the surface and the upper limit of the integral being 60 km. With σ given in $S\ m^{-1}$ and r in $\Omega\ m$, the column resistance per square metre column is in $\Omega\ m^2$. With V_i in V, J_z is in $A\ m^{-2}$. The integral of J_z

over the whole globe is equal to I_T . There is much greater variability in the column resistance, R , at any one location, than in R_T , due to variations in surface altitude, and local variations of aerosol concentrations and ion production by GCR flux, and other space particle fluxes that mainly affect the stratosphere. Consequently the current density, J_z , is also highly variable over the globe, in the range $1\text{--}6\ \text{pA}\ m^{-2}$ (Tinsley and Zhou 2006).

Between the concentric Earth and the upper boundary the column resistance, R , can be considered the sum of a tropospheric column resistance T and a stratospheric column resistance S which are variable in location and time. The three dimensional atmosphere consists of a continuum of column resistances in parallel. The thickness of the atmosphere between the upper (60 km) and lower (h) boundaries is only about 1% of the Earth’s radius, so the geometry for the global

circuit can be taken as plane-parallel. The subscripts on T and S in figure 1 refer to representative column resistances at equatorial, low, middle, high and polar latitude locations. Then Ohm's law gives J_z at any location as $J_z = V_i / (T + S)$. So any input that modulates any or all of V_i or T or S will also modulate J_z at that location.

There are only $\sim 5\%$ changes in T and S with the variability of the GCR flux at low latitudes, but much larger changes in T and particularly in S at high latitudes with 10–20% variations of the GCR flux, and several space particle fluxes varying by orders of magnitude there. These variations are discussed in section 2.2. T and S also depend on ion loss processes and ion mobility, and these are discussed in sections 2.3 and 2.4.

The basic Wilsonian hypothesis has been amply confirmed by simultaneous observations over the globe of electric field time variations due to the equipotential ionospheric potential variations (sections 4.1.1 and 4.1.2); by the constancy of J_z with altitude to above 30 km (Gringel *et al* 1986); and by the agreement with the theoretical models noted in section 1.

2.1.2. Additional generators; due to solar wind and solar UV inputs to the atmosphere. The relative velocity (V) between the solar wind plasma that flows outwards from the sun with embedded magnetic field (B) interacting with the 'stationary' conducting obstacle that is the Earth and its magnetosphere generates an electric field (i.e. the $V \times B$ electric field) that is responsible for additional potential distributions superimposed on the global ionospheric potential V_i . These superimposed potentials map down conducting magnetic field lines, and appear in the magnetic polar caps, where the ionosphere is electrically connected to the solar wind. As indicated in figure 1, this is within about 30° of the geomagnetic poles, i.e. poleward of $\pm 60^\circ$ geomagnetic latitude. This potential pattern has maxima and minima in the dawn and dusk segments of the polar caps, respectively, and entails horizontal electric fields and associated changes in the vertical electric fields that map into the atmosphere below. The product of the north–south component, B_z , of the solar wind magnetic field (interplanetary magnetic field or IMF) and the relatively constant solar wind velocity is responsible for the dawn–dusk potential difference of magnitude 30–150 kV across each polar cap, which is shown in figures 1 and 2.

Also, as indicated in figure 1, the east–west component B_y of the IMF leads to a potential difference appearing between the northern polar cap ionosphere and the southern polar cap ionosphere, with a magnitude that is typically a few tens of kilovolts, and with sign and magnitude that depend on the sign and magnitude of B_y (Tinsley and Heelis 1993).

Figure 2 shows the variation of ionospheric potential along a section in the magnetic meridian, for a dawn–dusk potential difference of 80 kV, corresponding to $B_z = -5.5$ nT. This is from the modeled compilation of satellite data by Hairston and Heelis (1990). Similar variations are given by Weimer (1996, 2001). The thick solid line is for $B_y = 7$ nT, and the thin solid line is for $B_y = -7$ nT for typical solar wind velocities. In the southern hemisphere the curves for positive and negative B_y are interchanged, i.e. the higher potential within the southern

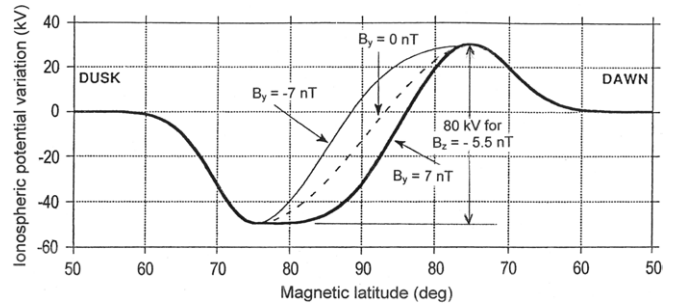


Figure 2. Ionospheric potential deviation from the 'global' value in the dawn–dusk magnetic meridian in the northern hemisphere with B_z negative; for an 80 kV total horizontal 'dawn–dusk' potential difference, and for three B_y values. In the southern hemisphere the variations correspond to those in the northern hemisphere but with the curves for positive and negative B_y interchanged.

polar cap is for B_y positive. The sign of B_y depends on whether the solar wind magnetic field points towards or away from the sun, and this polarity depends on the magnetic sector structure of the solar wind (Zhao and Hundhausen 1983) that rotates with the sun. Usually the sector structure is stable for a few months at a time, so that B_y changes from positive to negative usually occur with the 27-day rotation period of the sun. When a four-sector or six-sector structure replaces the simpler two-sector structure additional periodicities near 13 days or 9 days appear, with variable phase relative to the basic 27-day repetition.

The magnitude of the dawn–dusk (cross polar cap) potential difference and its spatial extension out from each magnetic pole depends on the level of geomagnetic activity. The extent can reach 40° magnetic colatitude (Hairston and Heelis 1990). At lower latitudes, at a given time, the ionospheric potential is normally constant except for perturbations of a few kilovolts, extending to the equator, due to the dynamo action of thermospheric winds moving plasma across magnetic field lines in the ionosphere. The winds result from diurnal solar UV heating of the thermosphere (the ionospheric dynamo, Richmond (1976), Roble and Hays (1979)). During magnetic storms additional global perturbations of the order of magnitude 10 kV are due to the dynamo action of winds due to auroral heating (the disturbance dynamo, Blanc and Richmond (1980)), and also to the downward mapping of magnetospheric electric fields (e.g. Anderson 2004). These potentials can be treated in models by the superposition of their values at any given time on the otherwise equipotential V_i at that time outside the polar caps.

2.2. Ion-pair production

As noted, the vertical column resistance R at any location is determined by the altitude of the surface and the resistivity r of the air as a function of altitude. The GCR flux creates ion pairs throughout the column, but the flux is severely attenuated below 15 km altitude. In the lowest 1–2 km above land surfaces, and extending over the oceans for a few hundred kilometres downwind from the continents, radioactive gases and aerosols originating in surface radioactive materials provide an additional source of ionization which usually dominates over the GCR source (Gringel *et al* 1986,

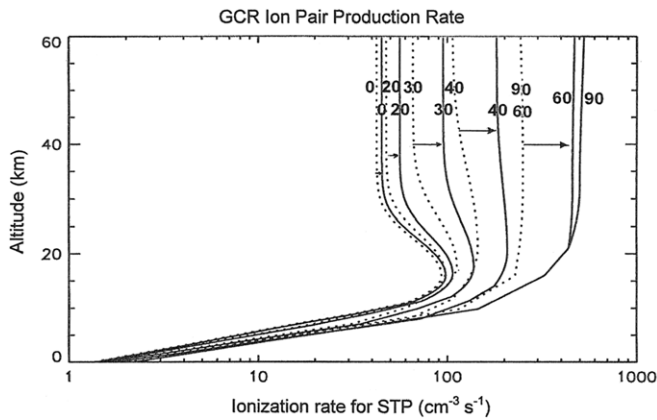


Figure 3. Variation in ion-pair production rate from galactic cosmic ray flux per unit volume of air calculated for STP air density, as a function of altitude for geomagnetic latitudes of 0° , 20° , 30° , 40° , 60° and 90° . The dashed lines are for solar maximum and the solid lines for solar minimum. The arrows indicate increases from solar maximum to minimum, which are a factor of two at high latitudes at the higher altitudes, but only about 5% near the equator.

Hoppel *et al* 1986). There are two further sources of ion-pair production; one is the relativistic electron flux and associated x-ray Bremsstrahlung that penetrates down to about 20–30 km in sub-auroral latitudes (Frahm *et al* 1997, Li *et al* 2001a, 2001b, Tinsley *et al* 1994), and the other is solar energetic particle, SEP, events (Holzworth *et al* 1987, Kokorowski *et al* 2006) that produce stratospheric ionization, excess positive charge, and occasionally a small amount of tropospheric ionization in the polar cap regions. In figure 1 the stratospheric and tropospheric contributions to the column resistance at any location are labeled S and T .

2.2.1. Ion-pair production due to the GCR flux. The flux of galactic cosmic rays into the atmosphere varies strongly over the globe, as the Earth's magnetic field acts as a geomagnetic latitude dependent barrier that prevents the penetration of these charged energetic particles, to an extent that depends on their gyro-radii in the geomagnetic (gm-) field. The gyro-radius depends on the magnetic rigidity (momentum per unit charge) of the particle. At gm-latitudes between about $\pm 60^\circ$ and the gm-poles, nearly all of the GCR particles, which have peak flux in the rigidity range 0.5–1 GV/nucleon, or for protons a kinetic energy of approximately 0.5–1 GeV, can reach the top of the atmosphere. At the gm-equator the gm-field produces a rigidity cut-off for vertically incident particles of about 15 GV.

Figure 3 shows the variation in ion-pair production rate as a function of altitude and gm-latitudes, based on the balloon-borne constant pressure ionization chambers of Neher (1967, 1971), and as parametrized by Tinsley and Zhou (2006), consistent with the parametrization of Heaps (1978) and observations of Morita (1983). At solar maximum the solar wind contains more magnetic irregularities than at solar minimum, and these act as a barrier for the propagation of GCR from the outer to the inner solar system. Thus at solar maximum the 1 GV/nucleon particles are reduced in flux by

about a factor of 3, and the 0.1 GeV/nucleon particles reduced by a factor of about 10 (e.g. Smart and Shea 1985).

These effects can be seen in figure 3, where the greatest solar cycle changes are at high latitudes and above 20 km altitude. There is little difference between the curves for 60° and 90° gm-latitudes at solar minimum, and none at solar maximum. The ionization rate is given per unit volume for air at STP. The actual ionization rate per unit volume is smaller by the ratio of air density at that altitude to the density of air at STP. The reason for the peak at about 15 km at low latitudes is the increased ionization by the secondary particle flux as the GCR particles lose energy, together with the lack of low energy GCR as a source of ion pairs between about 15 and 40 km.

There are changes in GCR flux on the timescale of a few days, known as Forbush decreases, which are due to solar coronal mass ejections that contain enhanced magnetic fields. As they pass beyond the Earth these attenuate the incoming GCR flux. The reductions vary in amplitude, but are comparable to the solar cycle changes. At high latitudes in the upper troposphere the ionization rate is decreased by up to about 20%, and for the low-latitude upper troposphere the variations are a factor of 3–5 smaller, as on the solar cycle.

Also associated with coronal mass ejections is the energization of trapped particles in the magnetosphere, which constitutes a 'ring' current as the ions and electrons drift in opposite directions around the Earth. This reduces the geomagnetic field strength out to several Earth radii, reducing the cut-off latitude for particles of a given rigidity, and by thus increasing the GCR flux for a given latitude, can oppose the effect of a Forbush decrease (Flückiger *et al* 1986).

On the timescale of multidecadal solar minima, the GCR flux increases above the solar minimum value, especially for rigidities 1 GV and below, by several times more than the increase from solar maximum to solar minimum. This energy range in protons is responsible for ^{10}Be production, and during the Maunder minimum (1650–1715 AD) there was an increase of about 100% in the ^{10}Be production (McCracken *et al* 2004).

2.2.2. Ion-pair production due to radioactivity. The atmospheric ionization due to radioactive materials in the ground is caused by direct α , β and γ radiation from the surface layers, and by radioactive gases (principally ^{222}Rn but also some ^{220}Rn) and their daughter products. Radioactive aerosol is produced by attachment of daughter products, and the ionization rate from radioactive gases and aerosol near the surface is up to 10 ion pairs $\text{cm}^{-3} \text{s}^{-1}$, depending on surface composition and porosity and the amount of vertical convection. Tinsley and Zhou (2006) used the data of Dentener *et al* (1999) for the geographical distribution of ^{222}Rn , with scale heights of 3 km in the local summer hemisphere and 2 km in winter. The geographical distribution of ^{222}Rn is affected by its half life of 3.8 days and the strength and direction of winds. The ion-pair production directly from the surface, including that from ^{220}Rn with its half life of 54 s, has a scale height of about 200 m, and is of order 10 ion pairs $\text{cm}^{-3} \text{s}^{-1}$ at land surfaces (Hoppel *et al* 1986). The ^{222}Rn is likely to be locally concentrated in updrafts of convective storms (Martell 1985) and although this is no

longer considered to be a significant (inductive) mechanism for thunderstorm electrification, it results in higher ambient conductivity below about 5 km, and enhanced J_z and charging at cloud boundaries.

2.2.3. Ion-pair production due to relativistic electrons and bremsstrahlung x-rays. In the middle stratosphere for sub-auroral to mid latitudes the ion-pair production due to relativistic (MeV) electrons precipitating from the quasi-trapped radiation belts in the magnetosphere can dominate over that due to GCR. Measurements of the flux at orbital altitudes, which determines the precipitating flux, with data on its variability in time and latitude have been made by Li *et al* (2001a, 2001b). These show a strong dependency of the flux on the solar wind velocity. At latitudes just equatorward of the auroral zone this flux is present most of the time, and it extends further into mid-latitudes with increasing solar wind velocity.

The precipitating MeV electrons are mostly absorbed in the atmosphere above 40 km altitude, but produce x-ray bremsstrahlung which can penetrate down to 25–30 km, and in the stronger precipitation episodes the ion-pair production rate can exceed that of GCR down to about 30 km (Frahm *et al* 1997). The GCR ion production normally maintains the column resistance of the stratosphere above 30 km small enough to be negligible in comparison with the column resistance of the troposphere. Thus, the addition of ionization by the relativistic electrons has little effect on the total column resistance or on J_z , except when the stratospheric column resistance increases for a few years following large explosive volcanic eruptions, which are inferred to produce a layer of ultrafine aerosol particles near 40 km altitude and poleward of latitudes of about $\pm 40^\circ$. Under these circumstances the changing relativistic electron flux can modulate the stratospheric column resistance and J_z (Tinsley and Zhou 2006). In particular, decreases of the flux for periods of a few days as the Earth passes through the low solar wind velocity region associated with the extension of the solar coronal streamer belt and the heliospheric current sheet (Kirkland *et al* 1996) can cause a decrease in J_z .

2.2.4. Ion-pair production by solar energetic particles. Particles of energy typically tens of megaelectronvolt coming from the direction of the sun have been found to increase in flux by many orders of magnitude following both solar flares and eruptions of solar coronal material into space. The events last from a few hours to a few tens of hours. They have been termed solar cosmic rays and solar proton events; however, since they contain small amounts of helium and heavier nuclei and electrons as well as protons, the term solar energetic particles (SEP) is preferable.

Most events have particle energy and flux sufficient to produce increases in ion concentration in the magnetic polar caps (where the geomagnetic field allows such low rigidity particles to enter) by several orders of magnitude at 50 km altitude, with smaller increases extending down to about 20 km. There are tens of such events per solar cycle, with occasional events where particles above several hundred MeV

are present with sufficient flux to produce some tropospheric ionization and neutrons that can be detected at ground level with high latitude neutron monitors. The effects on the global electric circuit include both large increases in stratospheric conductivity and the deposition of positive charge from the incoming positively charged atomic nuclei at mid-stratospheric levels. The positive space charge can then act as a temporary source of current density at high latitudes. Studies of the effects of large SEP events on the global circuit have been made by Holzworth and Mozer (1979) and Holzworth *et al* (1987), and a particularly comprehensive set of observations of the January 2005 events has been given by Kokorowski *et al* (2006).

2.3. Mobility of ions and local electric field

The processes that ionize the air produce electrons and positively charged molecules, with the electrons attaching to neutral molecules in microseconds, and then the positive and negative molecular ions growing in the next few milliseconds by attachment of trace polar molecules such as H_2O , NH_3 , H_2SO_4 and HNO_3 to become relatively stable air ions with lifetimes of an hour or so in relatively clean air.

As noted earlier, the local electric field in the atmosphere is given by $E = Jr$ where J is the current density and r is the resistivity. The resistivity is related to the conductivity σ by $r = 1/\sigma$. In microphysical terms, $\sigma = \sigma_1 + \sigma_2$ the sum of the positive and negative conductivities, where $\sigma_1 = \mu_1 n_1 e$ and $\sigma_2 = \mu_2 n_2 e$, with μ_1 and μ_2 being the mobilities of the positive and negative air ions of concentrations n_1 and n_2 , respectively, and e the elementary charge. Current densities J_1 and J_2 are carried by the positive and negative ions, respectively, so that

$$J = J_1 + J_2 = (\sigma_1 + \sigma_2)E = (\mu_1 n_1 + \mu_2 n_2)eE. \quad (1)$$

For the normal atmospheric situation in the absence of strongly electrified clouds, where the current densities and electric field are predominantly vertically downward, we consider the downward direction as positive. For horizontal stratification we can replace J and E by J_z and E_z .

The relationship between the mobility μ of an ion in air and its diffusion coefficient D is given to a good approximation by

$$\mu = De/(kT_A), \quad (2)$$

where k is Boltzman's constant and T_A is the absolute temperature (e.g. Chapman and Cowling 1970, McDaniel and Mason 1973). The value of D decreases with increasing mass of the air ion, and varies with altitude due both to pressure and temperature changes, and is evaluated more accurately by experiment than theory. Taking the form of the variations with pressure, P , and temperature as that experimentally determined for water vapor molecules, we obtain (e.g. Zhou and Tinsley 2007)

$$\mu/\mu_0 = (P_0/P)(T_A/T_0)^{3/2}(T_0 + S_C)/(T_A + S_C), \quad (3)$$

where μ_0 is the mobility at a reference atmospheric pressure P_0 and absolute temperature T_0 that decreases with increasing ion mass, and thus on the extent of the clustering of the polar molecules around the ion. The mobility is generally

less for positive air ions than for negative ones. S_C is Sutherland's constant, given as 120 K by Rogers and Yau (1989). Equation (3) is an improvement over the use of 'reduced mobility' which assumes only a simple inverse variation of μ with air density. However, neither treatment considers changes in the composition and number of the polar molecules clustered around the ion. With increasing absolute humidity the mobility decreases (Fujioka *et al* 1983). It also decreases with the growth of the clusters towards the size of ultrafine aerosol particles (Yu and Turco 2001) with increasing concentrations of volatiles such as NH_3 , H_2SO_4 and HNO_3 especially with decreasing temperatures. Thus there is some variability and uncertainty in the values of μ_0 which depend on the composition of the clustering molecules and the humidity. Widely used values are due to Bricard (1965) for a reference atmospheric temperature (288.15 K) and pressure (1013.25 hPa) are $1.4 \times 10^{-4} \text{ m}^2 \text{ V}^{-1} \text{ s}^{-1}$ for the mobility of positive air ions, and $1.9 \times 10^{-4} \text{ m}^2 \text{ V}^{-1} \text{ s}^{-1}$ for negative ions.

2.4. Ion loss processes

The air ions are lost by recombination with ions of opposite sign, and by attachment to aerosol particles of mass sufficiently great and mobility sufficiently small that as charged aerosol particles they make a negligible contribution to conductivity. They are also lost by attachment to charged aerosol particles of the opposite sign, which is a form of recombination.

Despite being large enough to have a negligible mobility, most aerosol particles are small enough in size so that they normally carry at most only single elementary charges. Assuming this is true for all particles, and in the absence of gradients in J_1 and J_2 , the concentrations n_1 and n_2 of the positive and negative air ions are given by the ion balance equations:

$$dn_1/dt = q_i - \alpha n_1 n_2 - \beta_1 S_0 n_1 - \gamma_1 S_2 n_1, \quad (4)$$

$$dn_2/dt = q_i - \alpha n_2 n_1 - \beta_2 S_0 n_2 - \gamma_2 S_1 n_2, \quad (5)$$

where q_i is the rate of production of ion pairs per unit volume due to all the sources described earlier; α is the ion-ion recombination coefficient; S_0 is the concentration of neutral aerosol particles; β_1 and β_2 are attachment rate coefficients for positive and negative ions, respectively, to the neutral aerosol particles; and γ_1 and γ_2 are the attachment rate coefficients for positive ions to negatively charged particles (concentration S_2), and negative ions to positively charged particles (concentration S_1), respectively. At equilibrium when dn_1/dt and dn_2/dt in (4) and (5) are equal to zero the production of ion pairs is balanced by their loss. We now discuss the recombination and attachment terms that contribute to this loss.

2.4.1. Ion-ion recombination. The coefficient α for ion-ion recombination depends on the species of ion involved, the air temperature and the density. For air ions in the atmosphere there are experimental values in the stratosphere (Rosen and Hoffman 1981, Arijis *et al* 1983, Morita 1983); a theoretical formulation by Bates (1982) and laboratory measurements by

Smith and Adams (1982). These three sets of results agree with each other only within a factor of 2. Possible reasons for the discrepancies are discussed by Tinsley and Zhou (2006) who favored the results of Bates (1982), which lead to the following expressions for the variations of α with temperature T_A and concentration of air molecules M (in units of $2.69 \times 10^{19} \text{ cm}^{-3}$) suitable for use in three altitude (z) ranges:

$$0 \leq z < 10 \text{ km} : \alpha = 6 \times 10^{-8} (300/T_A)^{0.5} + 1.702 \times 10^{-6} (300/T_A)^{-1.984} \times (M)^{-0.451} \text{ cm}^3 \text{ s}^{-1}, \quad (6)$$

$$10 \leq z < 20 \text{ km} : \alpha = 6 \times 10^{-8} (300/T_A)^{0.5} + 1.035 \times 10^{-6} (300/T_A)^{4.374} \times (M)^{0.769} \text{ cm}^3 \text{ s}^{-1}, \quad (7)$$

$$z \geq 20 \text{ km} : \alpha = 6 \times 10^{-8} (300/T_A)^{0.5} + 6.471 \times 10^{-6} (300/T_A)^{-0.191} \times (M)^{0.901} \text{ cm}^3 \text{ s}^{-1}. \quad (8)$$

2.4.2. Ion-aerosol attachment. The four attachment rate coefficients β_1 , β_2 , γ_1 and γ_2 are functions of aerosol particle size, temperature, pressure, and the mobilities of the positive and negative ions, and can be evaluated from the theory of Keefe *et al* (1968) and Hoppel and Frick (1986), who with Yair and Levin (1989) extend the theory to include larger particles with multiple charges in particle size distributions. In such cases, equations (4) and (5) the values of β and γ can be taken to represent effective attachment coefficients, and S_1 and S_2 the totals for the concentration of all positively charged aerosol particles and all negatively charged aerosol particles, respectively. Representative values of β and γ for particle radii 0.02, 0.04 and 0.10 μm at air pressures and temperatures representing altitudes of 2, 4 and 10 km are given by Zhou and Tinsley (2007), based on the Bricard (1965) mobilities and equation (3).

The balance equations for production and loss of the charged aerosol particles are

$$dS_1/dt = \beta_1 S_0 n_1 - \gamma_2 S_1 n_2, \quad (9)$$

$$dS_2/dt = \beta_2 S_0 n_2 - \gamma_1 S_2 n_1. \quad (10)$$

If gradients in aerosol concentration and turbulence and convection are sufficiently small so that local electrical equilibrium is attained, then $dS_1/dt = 0 = dS_2/dt$ and

$$S_1/S_0 = (\beta_1 n_1)/(\gamma_2 n_2), \quad (11)$$

$$S_2/S_0 = (\beta_2 n_2)/(\gamma_1 n_1). \quad (12)$$

The total aerosol concentration remains constant, and is the sum of the charged and neutral concentrations, so

$$S_T = S_1 + S_2 + S_0. \quad (13)$$

Data on the variability of S_T over the surface of the Earth in July and December can be obtained from the Global Aerosol Data Set (GADS 1998), with an analytical expression for the size distribution given by Hess *et al* (1998). The surface

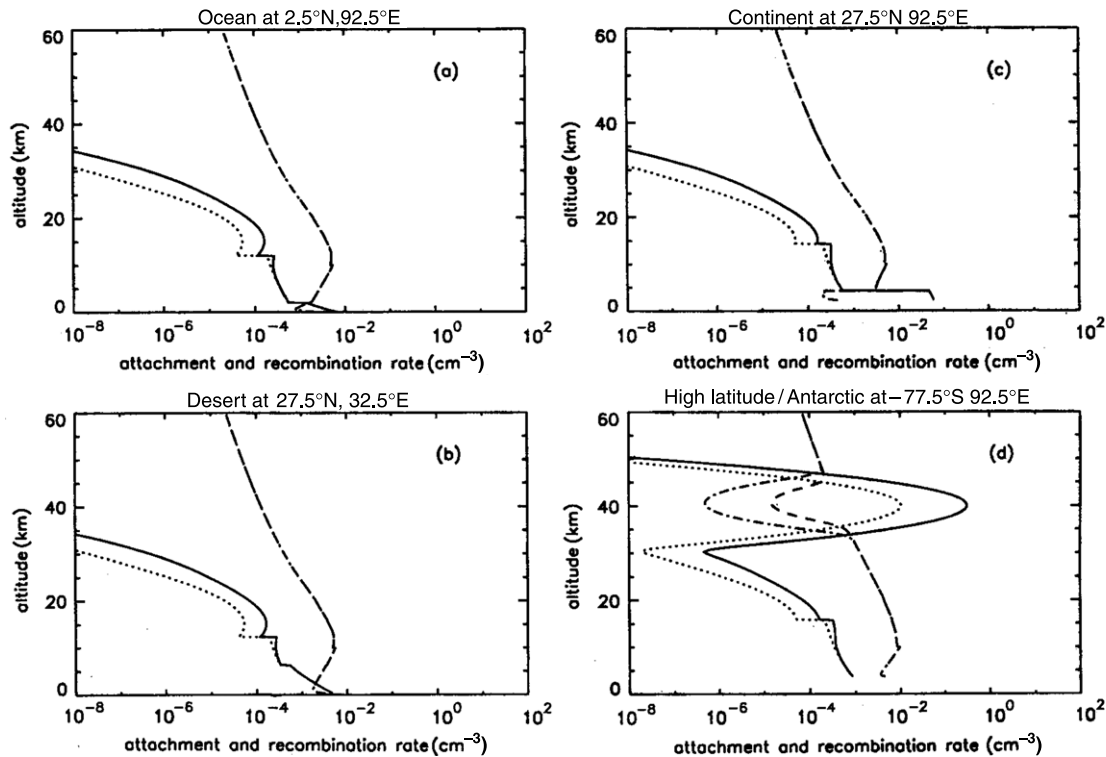


Figure 4. Vertical profiles for ion attachment rates $\sum \beta S_0$ to aerosols, and for the corresponding ion–ion recombination rate quantity αn , for four representative locations (a) ocean, (b) continent, (c) desert and (d) high latitude/Antarctic. The solid and dotted lines are for attachment with low and high volcanic aerosol concentrations, and the dot-dash and dashed curves are for ion–ion recombination with high and low aerosol concentrations, respectively. There is a layer of ultrafine aerosol particles at high latitudes that is enhanced by a factor of 30 with volcanic activity.

variations and examples of height profiles for various locations based on estimated scale heights are given by Zhou and Tinsley (2007).

Usually the β/γ ratios on the right of equations (11) and (12) are within a factor of five of unity, and n_1 within a factor of two of n_2 , so that S_T , S_0 , S_1 and S_2 at equilibrium are within an order of magnitude of each other. The time constant to achieve equilibrium values of S_1 and S_2 is $\sim 1/(\beta n)$ and can range from a few minutes, for higher altitudes where n is large (as is usual when S_T is small), to a few hours at low altitude where n can be very small, especially with larger S_T .

Additional aerosol components important for ion–aerosol attachment, but not detected optically, nor included in the GADS data, arise from ultrafine aerosol production due to nucleation from supersaturated, non-water volatiles, where concentrations of these are high enough and temperatures low enough, e.g. as observed by Seibert *et al* (2004). The nucleation may be by heterogeneous (neutral) processes (Curtius *et al* 2005), or by ion-induced nucleation (Yu and Turco 2001, Eisele *et al* 2006).

Ion-induced nucleation rates for H_2SO_4 with H_2O have been modeled by Yu (2002), and by Kazil and Lovejoy (2004), with the latter using experimentally determined rate coefficients (Lovejoy 2004) and obtaining different altitude profiles of production rates than Yu (2002). Ultrafine aerosol concentrations in the troposphere are not well known, and compared with the widely distributed particles characterized by the GADS data, are probably not important for attachment

of ions. However, a layer of ultrafine aerosols near 40 km altitude has been inferred to exist at mid-to-high latitudes, on the basis of measured H_2SO_4 mixing ratios in the lower stratosphere at low latitudes. The layer would be present for low levels of volcanic activity, but with ultrafine particle concentrations as much as 30 times higher for a few years after injections of SO_2 into the stratosphere by major explosive volcanic eruptions. The SO_2 is converted photochemically to H_2SO_4 , forming a lower stratosphere layer of larger particles, (e.g. Snetsinger *et al* 1987), which are carried by the stratospheric Brewer–Dobson circulation up to altitudes with high temperature that evaporates the liquid H_2SO_4 particles, then down into lower temperatures where the supersaturated vapor nucleates into ultrafine particles. The presence of H_2SO_4 vapor in the stratosphere also reduces ion mobility, as discussed in section 2.3.

Within the lowest few kilometres of the atmosphere the relatively high values of S_T and low values of n ensure that the rate of loss of ions by attachment (third and fourth terms on the right of (4) and (5)) exceeds that due to ion–ion recombination (second terms). Figure 4 is from Tinsley and Zhou (2006, their figure 8) and compares the loss rate for air ions due to attachment (βS_0) with the loss rate due to ion–ion recombination (αn) for four locations with different populations and height profiles of aerosols. Over the clean and high altitude Antarctic Plateau (figure 4(d)) the ion–ion recombination dominates at the surface; however, around 40 km the layer of ultrafine aerosol particles causes attachment

to dominate over ion–ion recombination even at that altitude, and even with low volcanic activity.

Turbulence or convection, especially at low altitudes, can move layers of charged aerosols and ions and radioactive ionization sources in times short compared with the time constant for equilibrium charging. Where $S_1 \neq S_2$ the result is irregular distributions in space and time of charged aerosols and ions and of net charge (space charge) and electric fields. This makes observations of the large-scale global circuit parameters very unreliable for land stations at low altitudes.

2.4.3. Ion attachment to droplets and large aerosol particles.

Where there are droplets or ice crystals or other large aerosol particles their size allows multiple charges to reside on their surfaces, with ions of both signs being captured rapidly. (The droplets also capture charged and uncharged aerosol particles at a much slower rate.) In the absence of an external electric field the ions diffuse from air to the surface of the droplets or particles, and with an electric field and its polarization of the droplet or particle, the drift currents J_1 and J_2 can further increase the rate of ion capture. The rate of charging of a droplet or large particle and the charge on it at equilibrium can be related directly to the size of the particle, the diffusion coefficients for the positive and negative ions, and the electric field. The average rate of capture of positive ions by a single droplet of radius A by diffusion only in the absence of an electric field is given by

$$G_{1,\text{dif}} = 4\pi AD_1 n_1 pc / (\exp(pc) - 1), \quad (14)$$

where p is the number of elementary charges on the drop (Fuchs 1934, Pruppacher and Klett 1997), and in SI units,

$$c = e^2 / (4\pi\epsilon_0 AkT_A). \quad (15)$$

Similarly, the rate of capture of negative ions is

$$G_{2,\text{dif}} = 4\pi AD_2 n_2 pc / (1 - \exp(-pc)). \quad (16)$$

The effect of an electric field E is to polarize the drop into a dipole and drive the conduction currents J_1 and J_2 , from opposite directions onto the drop, with its dipole charges and any net charge pe . The average rate of capture of positive ions due to E alone is given by Gunn (1956) and Pruppacher and Klett (1997) as

$$G_{1,E} = [\pi n_1 \mu_1 / (3EA^2)][3EA^2 - pe / (4\pi\epsilon_0)]^2, \quad (17)$$

and for capture of negative ions, with positive droplet charge pe

$$G_{2,E} = [\pi n_2 \mu_2 / (3EA^2)][3EA^2 + pe / (4\pi\epsilon_0)]^2. \quad (18)$$

The lifetime for ions when the dominant loss is to droplets can be obtained from (17) or (18) and is just a few seconds for typical clouds in the troposphere. The time constant for charging the droplets depends inversely on the products nD and $n\mu$ and can be less than a minute at high altitudes, to more than 20 min where n is low at low altitude and high aerosol concentration. The above equations can be generalized to treat a size distribution of cloud droplets (Pruppacher and Klett 1997) and ice crystals or large irregular aerosol particles, provided an effective radius is used to take into account the non-sphericity for such objects.

2.5. Production of space charge

2.5.1. Theory of boundary layer charging. As noted in the introduction, near the boundaries of clouds or aerosol layers there are large gradients in the droplet concentration, N , or aerosol concentration S_T , and thus large gradients in the ion concentration, atmospheric conductivity and resistivity. With a current density J flowing through a gradient of r , Ohm's Law gives a gradient of E , and Gauss's Law necessitates the production of space charge density ρ . The space charge appears in the form of differences in concentrations between the positively and negatively charged ions, the positively and negatively charged aerosol particles, and the positively and negatively charged droplets. With size distributions of aerosol particles and droplets we can express Gauss's Law as

$$\begin{aligned} \epsilon_0 \nabla \cdot E &= \rho \\ &= e(n_1 - n_2 + g_1 \sum S_1 - g_2 \sum S_2 + \bar{p} \sum N_A), \end{aligned} \quad (19)$$

where g_1 and g_2 are the mean number of charges on positively and negatively charged aerosols, respectively, and $\sum N_A$ represents a size distribution of droplets of radius A and \bar{p} is the mean charge on the droplets, given by $\bar{p} = (\sum p N_A) / \sum N_A$.

The presence of gradients in ion concentration introduces an additional term into each ion balance equation, on account of the divergence of the ion flows. For a total positive ion loss rate L_1 by recombination and attachment to aerosol particles and droplets, and a loss rate L_2 for negative ions, we can generalize (4) and (5) to become continuity equations

$$dn_1/dt = q_i - L_1 - (1/e)\nabla \cdot J_1. \quad (20)$$

and

$$dn_2/dt = q_i - L_2 + (1/e)\nabla \cdot J_2, \quad (21)$$

which means that a difference between production and loss can be made up by ions flowing into or out of the volume. The opposite signs applied to the divergences are due to the opposite directions of flow of the positive and negative ions that each constitute a positive J . Under steady state conditions with constant J , we have $\nabla \cdot J = 0 = \nabla \cdot J_1 + \nabla \cdot J_2$, with increase in J_1 accompanied by decreases in J_2 and vice versa. However, for the general case of varying dn/dt as in (4) and (5) J is no longer constant and

$$d\rho/dt = -\nabla \cdot J = -\nabla \cdot J_1 - \nabla \cdot J_2. \quad (22)$$

Thus equation (4), as a continuity equation for N droplets per unit volume of radius A , becomes

$$\begin{aligned} dn_1/dt &= q_i - \alpha n_1 n_2 - \beta_1 S_0 n_1 - \gamma_1 S_2 n_1 \\ &\quad - 4\pi N A D_1 n_1 pc / (\exp(pc) - 1) \\ &\quad - [\pi N n_1 \mu_1 / (3EA^2)][3EA^2 - pe / (4\pi\epsilon_0)]^2 \\ &\quad - (1/e)\nabla \cdot J_1, \end{aligned} \quad (23)$$

which is consistent with Griffiths *et al* (1974) for no gradient in concentration and pc small compared with unity, equivalent to the electrical potential of the charged droplet being small

compared with the thermal energy of the ions. Similarly, the continuity equation for negative ions becomes

$$\begin{aligned} dn_2/dt = & q_i - \alpha n_1 n_2 - \beta_2 S_0 n_2 - \gamma_2 S_1 n_2 \\ & - 4\pi N A D_2 n_2 p c / (1 - \exp(-pc)) \\ & - [\pi N n_2 \mu_2 / (3EA^2)] [3EA^2 + pe / (4\pi \epsilon_0)]^2 \\ & + (1/e) \nabla \cdot J_2. \end{aligned} \quad (24)$$

With the equations developed above, the concentration of ions and the charges on aerosol particles and droplets can be solved in several ways. The simplest solution is the equilibrium solution in the absence of space charge, i.e. with no gradients in droplet or aerosol properties, or the components of J , and therefore constant E . The equilibrium value of p for diffusion charging has been shown (Gunn 1954) to be

$$p = (1/c) \ln(D_1 n_1 / D_2 n_2), \quad (25)$$

where c is given by (15). The effect of the electric field charging (equations (17) and (18)) on the equilibrium value of p when in addition to diffusion charging, has been shown by Pruppacher and Klett (1997, section 18.3) to be given to the first order in γ as

$$p = (1 + \gamma/2)(1/c) \ln(D_1 n_1 / D_2 n_2), \quad (26)$$

where $\gamma = eEA/(kT_A)$ is a measure of electric field energy of the ions moving a droplet radius compared with their thermal energy. For $E < 2500 \text{ V m}^{-1}$ we have $\gamma < 1$, and so (26) is a reasonable approximation for weakly electrified clouds.

Thus equilibrium solutions can be obtained by solving (23), (24), (26), (19) and (22) with $d\rho/dt$ in (22) and the dn/dt terms in (4) and (5) set equal to zero, with specified values of temperature, pressure and ion production rate, with either J or E given and related by (1). Where size distributions of particles and droplets are present, S_T in (13) can be replaced by $\sum S_T$, and effective attachment coefficients used, and N replaced by $\sum N_A$ and A by its average \bar{A} to give an average constant \bar{c} from (15) and an average drop charge \bar{p} using (26). The diffusion and mobility D and μ are given by (2) with (3), and S_1 and S_2 or $\sum S_1$ and $\sum S_2$ in terms of S_T or $\sum S_T$ and n_1 and n_2 by (11), (12) and (13). Special cases of such equilibrium solutions are given for uniform conditions ($\rho = 0$) by Hoppel and Frick (1986) and with $S_T = 0$ by Griffiths *et al* (1974).

However, the presence of space charge in the form of additional charges on aerosol particles and droplets is of particular interest for the microphysics of clouds. In the boundary regions of clouds, or in general where there are gradients in the properties of clouds or aerosol layers, and with current density present, these cause gradients in electric fields, and values of $\nabla \cdot E$ and ρ and $\nabla \cdot J_1$ and $\nabla \cdot J_2$ that are no longer zero.

2.5.2. Results of models of cloud charging. For a horizontally stratified atmosphere the use of (19) with non-zero ρ is needed. The equilibrium solutions that are illustrated in figure 5, from the model of cloud charging by Zhou and Tinsley (2007), are based on the assumption that the droplet charging due to the electric field (equations (17) and (18)) was negligible compared with diffusion charging (equations (14) and (16)). This is a

reasonable assumption for most clouds; however, the terms for the electric field charging may be needed for clouds near sea level (low conductivity) and with large average droplet radii and concentrations.

The reduction of the mobility of air ions with increasing humidity inside and around clouds, or within supersaturated stratospheric layers of H_2SO_4 vapor, as discussed earlier, has not been introduced into models, and it is expected to have a non-negligible effect.

Solutions that are time dependent for the concentrations of ions and charged droplets and aerosol particles can be made in several ways. For horizontal stratification and given temperature and pressure and aerosol and droplet and size distributions as a function of altitude one can begin with zero values of n_1 , n_2 , S_1 , S_2 , and p , and then with given values of q and J_z allow the numerical simulation of the charging process to take place.

An alternative and more realistic time-dependent solution for processes in clouds would be to begin with a solution for S_1 and S_2 with specified q and J_z and other parameters, but zero $\sum N$ and p , and then have the latter two increase in time. The gradient of the electric field depends on the gradient of conductivity, so it is necessary to model the whole boundary region from outside the cloud to where the droplet concentration is constant inside, to determine the variation of E .

A set of time-dependent solutions to cloud boundary charging was obtained by Klett (1972) for electric fields, constant in time, that originated within the clouds, and with no ion production in the cloud ($q = 0$) and thus no current density J_z continuous in space or time, and no aerosols ($S_T = 0$) and a boundary layer of zero thickness, and only diffusive charging of droplets. He modeled screening layers of space charge, which formed in less than a minute, and penetrated a few metres in from the sharp edges of the clouds.

The time constants for droplet charging and aerosol charging with ambient ions can range from minutes to hours. Since space charge is created in initially non-electrified clouds when the current density J_z moves charges from one region to another, an overall time constant for producing a space charge layer can be evaluated by considering the integrated change in electric field over the thickness of the boundary layer. This is an effective surface charge, which can be related to the change in electric field, depending on change in conductivity from outside (σ_{out}) to inside (σ_{in}) the cloud. Then the surface charge divided by J_z gives the overall time constant τ_0 for charging the layer; giving $\tau_0 = \epsilon_0(1/\sigma_{\text{out}} - 1/\sigma_{\text{in}})$. With typical conductivities of $10^{-12} \text{ S m}^{-1}$, $10^{-13} \text{ S m}^{-1}$ and $10^{-14} \text{ S m}^{-1}$ for air outside a cloud at 10 km, 4 km and 2 km (with continental aerosol), respectively (Tinsley and Zhou 2006), the reduction of conductivity by a factor of 10 going into a cloud gives charging times of $\sim 1 \text{ min}$, $\sim 10 \text{ min}$ and $\sim 2 \text{ h}$, respectively.

These charging times are comparable to typical convection and turbulence characteristic times, and they point to the need to construct time-dependent cloud and aerosol charging models that include turbulence and convection. The presence of downdrafts at cloud tops and updrafts at cloud base can

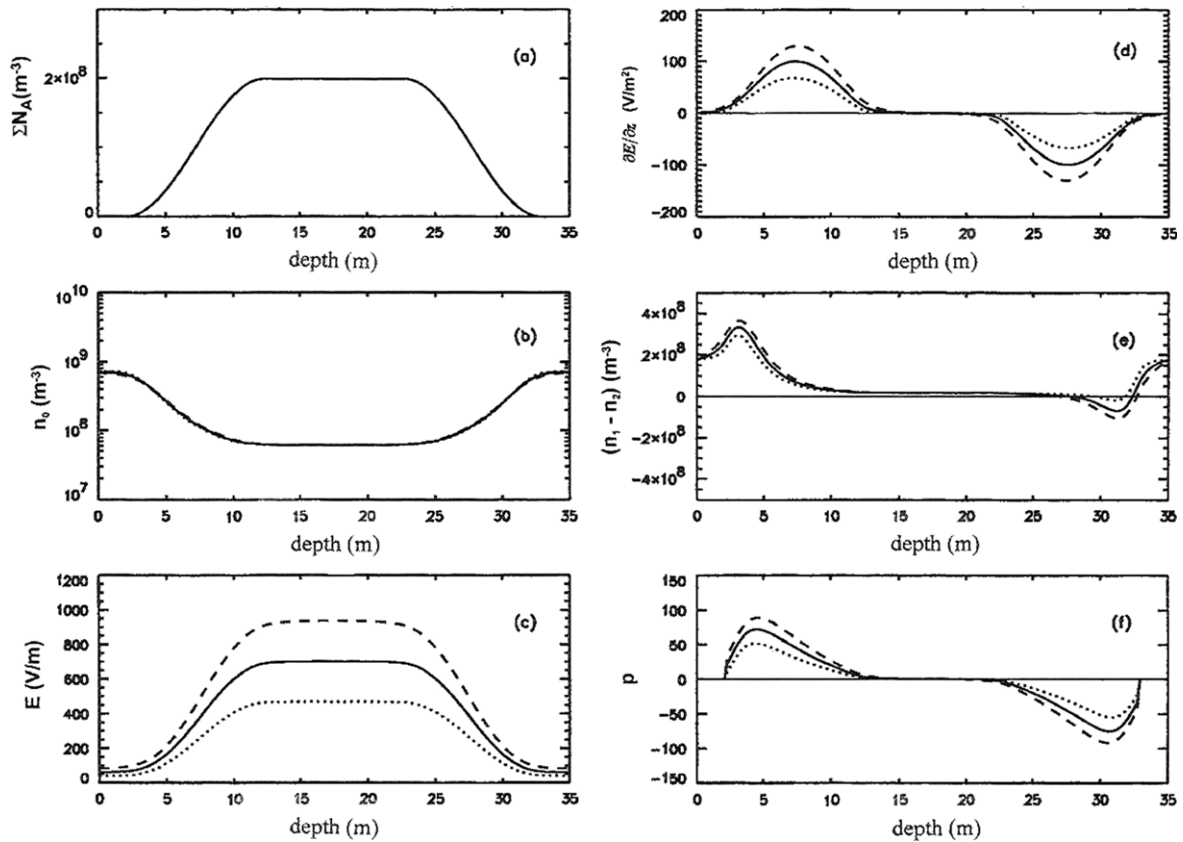


Figure 5. Plot of cloud parameters as a function of depth with upper and lower boundary regions 10 m thick and uniform interior 11 m thick and 2 m air layers above and below the cloud. The cloud is at 4 km altitude and the droplet concentration (a) is $2 \times 10^8 \text{ m}^{-3}$ at maximum, producing an associated drop in ion concentration (b). The electric field (c) depends on the current density J_z , and the dashed line is for $4 \times 10^{-12} \text{ A m}^{-2}$; the solid line is for $2 \times 10^{-12} \text{ A m}^{-2}$; and the dotted line is for $1 \times 10^{-12} \text{ A m}^{-2}$. The electric field gradient (d) determines the space charge on the ions (e) and the droplets with mean positive number of charges p shown in (f), with line types for the same values of J_z as used in (c). Space charge on the aerosols is intermediate between that for ions and droplets and is not shown. The thin solid lines are zero references. From the same model as used by Zhou and Tinsley (2007).

increase the macroscopic electric fields and current densities, by injecting a tongue of higher conductivity air onto a lower conductivity layer, and it can also thin a boundary layer, and both effects can enhance the space charge and droplet and aerosol charging. Turbulence in general would decrease the peak concentration of space charge, but would create a larger irregular volume containing charge. A comparison of model results with observations is given in section 5.1.

3. Modeling the dc properties of the global circuit

With the global circuit fundamentals described in the previous section, it is possible to construct models of atmospheric ion concentration and conductivity as a function of altitude and location over the globe, and to evaluate the column resistances from the surface to the ionosphere over the globe. Then measurement of some parameter that allows the output of the generators to be determined, e.g. a vertical profile of atmospheric electric field (often denoted by its negative value, the potential gradient, PG, which is positive upwards) at one, or preferably an ensemble of locations outside the polar caps, allows the ionospheric potential V_i for that time to be determined. A separate determination of the superimposed potential distribution within the polar

caps is also required, and that can be inferred from spacecraft measurements expressed as fitted models as functions of solar wind parameters (section 2.1.2).

The determination of ionospheric potential normalizes the model to a distribution of current density over the globe, and to a total charging current I_T . This normalization is valid for the time of the V_i determination only, as there are important time variations of V_i , and important time variations in the distribution of column resistance, especially with geomagnetic latitude as a function of solar activity, and also regionally with changes in volcanic and other natural aerosol populations, and with anthropogenic aerosols.

3.1. Results of a global circuit model

The model of Tinsley and Zhou (2006) includes only the changing GCR flux and changing distribution of aerosols. The tropospheric aerosol changes from June to December make only a small difference to the tropospheric column resistances. A large effect is due to the estimated amounts of ultrafine aerosol particles in the stratosphere, for a few years following large increases in the mixing ratio of H_2SO_4 there, as a result of large explosive volcanic eruptions. Figure 6 shows results from the model, in the form of column resistances R along two

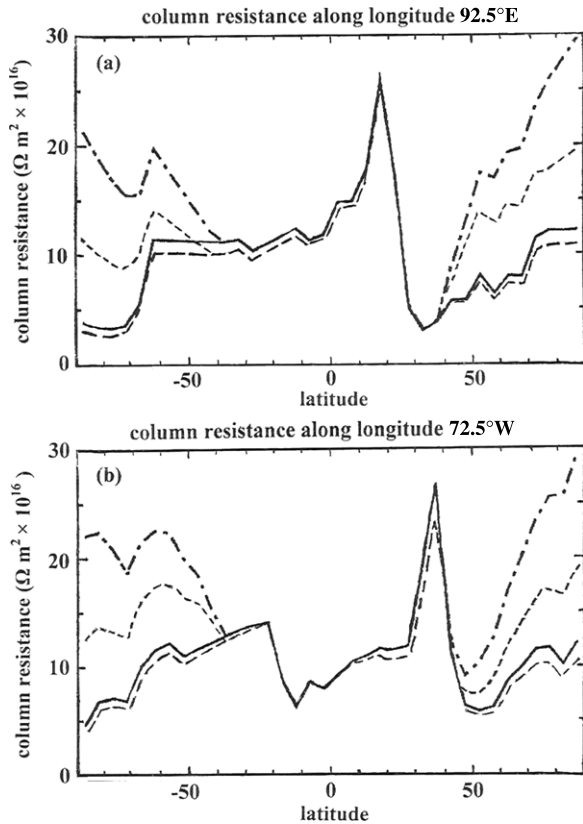


Figure 6. Profiles of column resistance R along (a) longitude 92.5° E and (b) 72.5° W. The curves are for December conditions, with no stratospheric ion production by relativistic electrons. The solid curves are for solar maximum (cosmic ray minimum) and the large dashed curves for solar minimum, both in the absence of stratospheric ultrafine aerosols. The dotted-dashed curves are for solar maximum and the small dashed curves for solar minimum, in the presence of stratospheric ultrafine aerosols. For details see Tinsley and Zhou (2006).

meridional sections, one at longitude 92.5° E (East Asian) and the other at 72.5° W (the Americas). For each of the longitudes the curves for solar maximum and minimum are shown for situations with and without the estimated stratospheric ultrafine volcanic aerosol layer. The variable precipitating relativistic electron flux (section 2.2.3) was not modeled, and when present it greatly reduces the effect of the stratospheric ultrafine aerosols.

In figure 6 the solar cycle variation of cosmic ray flux and R is only a few per cent near the magnetic equator, which with the centered tilted dipole model, and at 72.5° W longitude, is near 12° S latitude. At 92.5° E longitude it is near 12° N latitude. The peaks in column resistance are due to polluted industrial regions near sea level in each case, and the minima in column resistance correspond to the clean high altitude Antarctic plateau and Himalayas. Near the magnetic poles the solar cycle variation of R is about 20% in the absence of stratospheric volcanic aerosols, but can be above 50% with the estimates for the stratospheric ultrafine aerosol layer, in the absence of relativistic electron precipitation.

Summing the reciprocals of all such column resistances (i.e. summing the conductance for each column) one obtains a value for the global atmospheric conductance and its reciprocal

the global load resistance R_T . The results for the mean July–December values for minimal volcanic activity were 182Ω for R_T for solar minimum and 196Ω for solar maximum, which is a 7% variation over the solar cycle. For maximal volcanic activity the values are 217 and 242Ω for a 12% solar cycle variation. The latter figure is higher on account of the greater percentage change of the GCR flux in the stratosphere, modulating the column resistance of the stratospheric ultrafine aerosol layer at mid-high latitudes.

Normalizing the model to a variety of observational data sets on J_z , using model values of R at the location and time of the J_z observations, the total charging current I_T was calculated to be in the range 1000–1600 A, and the ionospheric potential V_i in the range 180–300 kV. There is more variability and uncertainty in evaluating I_T and V_i than in R_T because of the much greater variability in I_T , on diurnal and interannual and solar cycle and longer timescales. The solar cycle and longer term variations in I_T are uncertain even in sign, as will be discussed in section 4.

3.2. Modifications and additions to models

3.2.1. Effects of clouds. Clouds and water vapor introduce regions of lower conductivity into an atmospheric column, and their effect on column resistance, especially for low clouds of larger droplet radii, is important. Low clouds cover about 30% of the Earth’s surface, and when middle and high clouds are included, the average total cloud cover is about 70% (Rossow and Lacis 1990). The requisite input data for inclusion of their effects in models is now becoming available from aircraft observations of droplet size distributions and spacecraft observations, such as from the ‘A-train’ of Earth observing spacecraft, that include the altitudes of the upper and lower cloud boundaries and moisture profiles (Stephens *et al* 2002).

3.2.2. Effect of polar cap and other superimposed potential patterns. As noted in section 2.1.2, there is a superposition of potentials originating from the solar wind interaction with the Earth, which perturb the ionospheric potentials in the northern and southern polar cap regions. Parameters describing these patterns are a function of the solar wind velocity and IMF components, and measurements with spacecraft both in the polar cap ionospheres and in the solar wind allow empirical models, such as those of Hairston and Heelis (1990) and Weimer (1996, 2001) to relate the potentials to the solar wind parameters. Then, using measured solar wind parameters for a given time as input to the model, the perturbations to V_i and J_z and E_z for that time can be modeled as a function of coordinates such as magnetic latitude and magnetic local time, followed by a coordinate transformation to geographic coordinates. Similar superpositions can be made for the potential patterns of the ionospheric dynamo, the disturbance dynamo and magnetospheric electric fields.

3.2.3. Effect of stratospheric ultrafine aerosols. As noted in sections 2.4.2 the conductivity in the middle and upper stratosphere is decreased by the presence of ultrafine aerosol particles. The enhanced stratospheric ultrafine aerosol layers

persist for a few years after the large explosive volcanic eruptions that inject SO_2 into the stratosphere (Bingen *et al* 2004, Deshler *et al* 1993), and appear capable of making the stratospheric column resistance values for those years for mid/high latitudes comparable to the tropospheric column resistance values (Tinsley and Zhou 2006). Only small effects are likely to be present in the periods between volcanic eruptions, as the H_2SO_4 mixing ratio in stratospheric air falls to a background of about 3% of the high values following eruptions. Variability in the ultrafine aerosol distribution due to atmospheric dynamics may be part of the explanation for the anomalous values of stratospheric conductivity measured by balloons (Byrne *et al* 1988, Rosen and Hoffman 1988, Hu and Holzworth 1996, Ermakov *et al* 1997).

A large improvement over the estimates of Tinsley and Zhou (2006) for the ultrafine particle production is possible if actual values of H_2SO_4 and H_2O mixing ratios in the descending branch of the Brewer–Dobson circulation are determined, and utilized together with a model of the nucleation mechanism for the actual stratospheric temperatures and pressures and ion concentrations. A time-dependent model treating the Brewer–Dobson transport, together with turbulence and wave activity may be necessary to adequately model the particle growth and coalescence processes.

3.2.4. Effects of relativistic electron precipitation. The stratospheric conductivity is also strongly affected by the production of ionization due to the precipitation of relativistic electrons and the bremsstrahlung x-rays that they generate. The ion-pair production due to such relativistic electron precipitation at sub-auroral latitudes was modeled for two specific events by Frahm *et al* (1997). To adequately model effects on the global circuit for a few years following volcanic eruptions, the time and latitude variations (e.g. as observed by Li *et al* 2001a, 2001b) of the energy spectrum of the precipitating electrons is required, preferably expressed as a function of solar wind parameters. The transition from a solar wind sector with IMF direction ‘towards the sun’ to one that is ‘away from sun’ is called a heliospheric current sheet (HCS) crossing. A reduction in the flux of precipitating relativistic electrons is observed for a few days at HCS crossings. Then using measured solar wind parameters, both the reductions of the flux at HCS crossings (as illustrated by Kirkland *et al* (1996, their figure 7) and Kniveton and Tinsley (2004, their figure 1)) as well as the solar cycle variability can be modeled. Then models such as those of Frahm *et al* (1997) can be constructed for a range of mid-high latitudes, utilizing the above flux data as inputs, to evaluate the ion-pair production in the stratosphere.

4. Global circuit time variations from internal and external inputs

Variability in the parameters of the global circuit can occur on all time and spatial scales. There are two main types of variability that are reflected in J_z changes. The first is due to variability of the global charging current to the ionosphere I_T , with the resulting change in V_i . The second is in the distribution

of atmospheric conductivity, mainly with GCR changes, but with smaller effects of aerosols (especially from volcanic eruptions) and of space particle fluxes other than GCR.

4.1. Diurnal through solar cycle variations

4.1.1. Diurnal and annual I_T generator inputs. The diurnal variation of the PG near the Earth’s surface was the first variation to be clearly established. Measurements at sea (Torreson *et al* 1946) in different oceans showed that the variation (called the Carnegie curve) was a function of universal time rather than local time, thus pointing to global variations of ionospheric potential. Consistent with the Wilson (1920) hypothesis, the total global current output of thunderstorms and of highly electrified clouds, which predominate in afternoon and evening local times in the irregularly spaced land masses of Africa and the Americas and the Australia/Indonesia region, generate the universal time variation as these land masses rotate under the sun. Contributions from oceanic thunderstorms are a minor part of the global output (Williams 2005). The land masses at low latitudes are not symmetrically distributed between the northern and southern hemispheres, and convective activity predominates in the local summer months, so both the mean output and the shape of the diurnal curves show an annual variation. The analysis of Adlerman and Williams (1996) showed a maximum of monthly average PG in the northern summer months, consistent with more land masses at low latitudes in the northern hemisphere than in the southern. A comprehensive set of high quality PG measurements from Vostok, on the Antarctic plateau, was analyzed by Burns *et al* (2005), which confirmed that the May through August average was 20% higher than the November–February average.

The Vostok data also showed changes in the shape of the diurnal curves through the year. For November–February the diurnal range was about $\pm 30\%$ of the mean, while for May–August the range was about $\pm 15\%$. There was also a shift in the time of the peak from near 1830 UT in November–February to near 2030 UT in May–August, consistent with the more westerly longitudes of the low-latitude parts of the Americas and Africa in the northern as compared with the southern hemisphere. The larger percentage variation for November–February is because of a deeper minimum that may be due to less land in the southern hemisphere around the longitudes for generating summer thunderstorms at the UT of the minimum.

4.1.2. Day-to-day I_T generator inputs. Diurnal variations of PG measured on land at other than high mountains show a great deal of day-to-day variability that is due to variations in conductivity and space charge as aerosol layers and radon concentrations are perturbed by turbulence and convection, even in ‘fair weather’ in the absence of clouds. Thus they usually measure local rather than global diurnal variations, especially when there are regular diurnal variations of convection. At sea and from high mountains and from aircraft the amplitude of conductivity and space charge variability is reduced, but the Carnegie curve and later confirmations of it required averaging of many days of data. A comparison of

4 h averages of PG measurements in September 1928 made simultaneously at Eskdalemuir, Scotland, and at sea in the western Atlantic (Torreson *et al* 1946) showed only a moderate correlation (0.56) in a selected period of five days (Harrison 2004b). Higher correlations were found in simultaneous balloon flights from southern Germany and the equatorial Atlantic (Mühleisen 1971) and from simultaneous aircraft flights separated by 1400 km (Markson 1985).

Measurements of current density J_z should be less susceptible to local effects, but the instruments have proved difficult to operate and calibrate. The ice plateaux of Antarctica and Greenland are excellent surface sites for observing PG and J_z changes that show global variations, as the sites combine minimal aerosol and negligible radioactivity with minimal convection and turbulence on the cold uniform ice surfaces, with high conductivity from the altitudes and geomagnetic latitudes that more quickly dissipates the minimal space charge. The ice plateaux PG observations show day-to-day variability (Bering *et al* 1988, Tinsley *et al* 1998, Burns *et al* 2006, figure 1), with standard deviation of daily averages about 10%, which is most likely due to the variability of the low latitude, highly electrified cloud generators. There are certainly day-to-day meteorological changes in the three main generating regions, which can account for day-to-day changes in the shape of the diurnal curves and their mean diurnal averages, for I_T and V_i , and the consequent measured J_z and PG values.

4.1.3. Day-to-day solar and 27-day solar inputs. There are disturbances on the sun lasting from hours to months that are associated with regions of strong magnetic field in its outer layers. The sun's rotational period increases from solar equator to poles from 25 to 29 days, but most of the disturbances originate at middle solar latitudes with a period of about 27 days, and so the day-to-day disturbances to the global circuit caused by solar emissions propagating to earth also show 27-day periodicities. The solar UV emissions show variability on the day-to-day timescale, and also show an increase in mean level and 27-day variability near the maxima of the 11-year sunspot cycle. The ionospheric heating and winds maximize in summer at mid-latitudes, and this and the solar variations are carried over into the electric and magnetic field variations associated with the consequent ionospheric dynamo. The diurnal (local time) magnetic field variations have been long studied (Matsushita and Maeda 1965) but the superimposed variations in V_i , and J_z and PG values are only a few per cent of the variable daily average V_i values, and have yet to be identified.

Variations occur also in the solar wind, on all time scales from hours to decades, and these appear at all phases of the solar cycle. There are several ways in which these perturb the global circuit. In the polar caps a solar wind with an ideal two magnetic sector structure and two HCS crossings per solar rotation would produce a 27-day square wave in the IMF B_y and in the associated perturbation of V_i as described in section 2.1.2 and figure 2. An ideal 4- or six-sector structure would produce square waves of period 13.5 or 9 days. Examples of the changes in PG at HCS crossings measured

at Vostok on the Antarctic plateau, and their relation to an empirical model of satellite measurements are given by Burns *et al* (2006, figures 2 and 3).

The IMF B_z component causes dawn–dusk potential differences across the polar caps. During geomagnetically quiet times (e.g. as characterized by low values of the geomagnetic index K_p) the potentials on the dawn side are 20–30 kV higher than on the dusk side, while during geomagnetic storms (large negative B_z , and/or large K_p) the dawn–dusk potential difference increases to 150–200 kV (Boyle *et al* 1997). The corresponding change in overhead ionospheric potential for high latitude surface stations has been observed as a diurnal variation in PG superimposed on the ‘Carnegie curve’. A separation of the solar-wind-induced diurnal variation from the this internally generated diurnal variation was made for such stations as a function of K_p by Pumpyan *et al* (1987) and by Burns *et al* (1995), and as a correlation with an empirical ionospheric potential model by Tinsley *et al* (1998) and Burns *et al* (2005).

At the distance of the Earth from the Sun an HCS is usually associated with a drop in solar wind speed for a few days (e.g. from 470 to 410 km s⁻¹ in the data of Tinsley *et al* 1994, figure 5). The slower solar wind speed reduces the population of relativistic electrons partially trapped in the Earth's radiation belts (Li *et al* 2001b). Loss into the atmosphere of these quasi-trapped particles occurs, but only at sub-auroral latitudes—outside the polar caps—because inside the polar caps the field lines are open to the solar wind, and do not allow quasi-trapping. In years of high stratospheric aerosol loading the reduction in stratospheric ionization from the reduction in relativistic electron precipitation at HCS crossings accounts for the reduction in PG seen at such crossings by Fischer and Mühleisen (1980) and Reiter (1977) (also see section 2.2.3 and Tinsley *et al* 1994).

The effects of SEP events, as discussed in section 2.2.4, are confined to within about 30° colatitude from the magnetic poles, and events large enough to significantly perturb J_z at those latitudes occur at most only a few times per year. The short-lived effect on the global circuit has been modeled by Tzur *et al* (1983), and they discuss the deposition of positive space charge in the stratosphere by the incoming large fluxes of positively charged atomic nuclei. The effects on the global circuit last only a few hours at high magnetic latitudes, and are strongest in the stratosphere, where the conductivity can increase by an order of magnitude or more and the vertical field at these altitudes can decrease to near zero (Kokorowski *et al* 2006).

The decreases in GCR flux known as Forbush decreases (FDs) are usually detected as reductions in neutron monitor count rates; they have amplitudes of 5–10%, and occasionally up to 20% of the undisturbed levels; and usually have onset time less than a day, with a slow recovery lasting about a week. The changes in GCR energy spectrum are similar to those on the 11-year solar cycle, producing a similar geomagnetic latitude variation in ion-pair production. Measurements of the effects of FDs on PG have been made from a low altitude land site by Márcz (1977). FD effects have been modeled by Tzur *et al* (1983) and Sapkota and Varshneya (1990), with the global

ionospheric charging current I_T assumed constant during the events, but it is not clear at present whether this is a good approximation.

The FDs are associated with coronal mass ejections with their embedded magnetic fields passing across the Earth on their way to the outer solar system, which attenuate the incoming GCR flux with decreasing effectiveness as they recede and expand. They are sometimes, but not always, preceded by solar flares, and those with negative IMF B_z are likely to initiate magnetic storms. Solar flares are often, but not always, followed by FDs and/or magnetic storms. The observations by Cobb (1967) and Reiter (1969) showed PG and/or J_z changes at mountain observatories associated with solar flares. Their data can be taken as a mixed response to SEP events, FDs, ring-current related changes of rigidity cut-off latitude for the GCR flux, and the ionospheric disturbance dynamo.

Aircraft measurements of PG made over many years show Carnegie curve diurnal variations (Markson 1976, 1985) and day-to-day changes of the extrapolated V_i , which have been attributed to changes in the solar wind velocity that affect the GCR flux (Markson and Muir 1980, Markson 1981). Markson (1981, 1986) made a 'crude estimate' that a 10% variation in the GCR flux (as measured by a high latitude neutron monitor, or by related measurements on a spacecraft) was accompanied by a 10–20% increase in ionospheric potential measured in the Bahamas. Since the Bahamas are at low latitudes where changes in cosmic ray flux and therefore conductivity would be only 20% or so of those measured by the neutron monitor (e.g. Tinsley and Zhou 2006), we are left with the inference that an increase in global thunderstorm current output (I_T) was responsible. If so, it is puzzling that there is such a large percentage increase in the current output for a 10% GCR change at high magnetic latitude, unless, as implied by Markson (1986) the output depends on the 4th or 5th power of the change in conductivity in and above cloud tops. However, the time interval of the Bahamas observations was only a few months, and much of the correlation could be due to unrelated trends in V_i and the GCR flux. So an important issue remains to be resolved—how much of the day-to-day variability in I_T and in V_i is due to meteorological changes affecting the convective activity that produces highly electrified clouds, and how much is due to the changes in the electrical output of such clouds due to changes in conductivity in and above cloud tops due to external ionizing inputs.

4.1.4. Interannual, volcanic and solar cycle inputs. Fischer and Mühleisen (1972, 1980) made a large set of PG measurements as a function of altitude from balloons, mostly over South Germany, and from them inferred V_i values for 1959–1976. Together with Markson (1981, 1986) and Meyerott *et al* (1986) they have discussed the year-to-year variations in the context of solar cycle and volcanic influences. From less than two solar cycles and one large volcanic event (Mt. Agung in 1963) that loaded the stratosphere with sulfate aerosol, no clear result emerged. There is a suggestion for a possible inverse relation between V_i and sunspot number (a 15–20% increase in V_i from solar maximum to solar

minimum, i.e. a positive correlation with GCR flux, and also an increase in V_i associated with the increase in stratospheric volcanic aerosol load. However, further determinations of V_i through 1984 by Markson (1985) failed to show a continuation of the inverse correlation with sunspot number.

An indirect inference of a solar cycle variation of V_i for the period 1966–1982 is due to Olson (1983) who measured J_z with balloons in the stratosphere, mostly over Lake Superior. He found a 30–40% increase in J_z from the 1969 solar maximum to the 1976 solar minimum, partly due to the decrease in column resistance at that latitude with increasing GCR flux. From the model of Tinsley and Zhou (2006) the column resistance decrease would be about 10%, so that the remaining 20–30% increase in J_z again suggests an inverse relation between sunspot number and V_i , at least from the 1960s to 1976.

Earlier in the 20th century the observations that were available were from noisy low altitude land surface stations, with only a small fraction of fair weather days, and problems due to varying conductivity, with local radioactivity and aerosols. The observations seem to suggest (Bauer 1925, Israël 1961/1973) that up to the middle of the century the relation of V_i to the sunspot cycle consisted of a V_i maximum at solar maximum, i.e. the opposite of the later variation. Atmospheric nuclear tests in the late 1950s and early 1960s caused large perturbations then, masking any global signal.

An analysis of 20th century PG and J_z trends for a number of land surface stations in the general area of northern Europe has also been made by März and Harrison (2005), and a trend to decreasing PG and J_z over much of the 20th century was inferred. It may be due to the trend of decreasing GCR flux affecting the thunderstorm generators, and/or to changes in environmental conditions at the sites.

One should expect interannual variations in V_i due to climate cycles, such as El Niño, affecting sea and land surface temperature and humidity, and thus thunderstorm output, and these may be masking (or giving false appearances of) solar cycle effects on V_i . It seems that long term (multidecadal) and well calibrated observations of PG and J_z from high quality sites are needed to clarify the effects of volcanoes, the solar cycle, and climate cycles on V_i . Such sites are available on the Antarctic and Greenland ice plateaux, in Tibet and in the Andes, and on oceanic or otherwise clean, low humidity, high mountain locations.

4.2. Long term variations

4.2.1. Century and extended solar minima inputs. During some intervals lasting several solar cycles or more the sun has been observed to have very few sunspots. The most notable of these multidecadal extended solar minima was the Maunder minimum (ca 1650–1715 AD). During the shorter Dalton minimum (ca 1795–1825) the maximum sunspot number was only about a third of the maximum numbers before and after. Cosmogenic isotopes (e.g. ^{14}C and ^{10}Be) in tree rings, ice cores and lake and ocean sediments are a proxy that shows enhancements in the incoming GCR flux at these times, with greater enhancements associated with fewer sunspots and

longer durations of the minima. As noted in section 2.2.1, McCracken *et al* (2004) found that during the Maunder minimum in the polar regions the lower energy GCR that produce ^{10}Be increased by about 100% relative to present mean values, which is several times larger than the present solar cycle variation.

While the amplitude of the sunspot cycle shows characteristics of chaotic processes, periodicities of about 90 and 200 years appear in both the sunspot and the cosmogenic isotope record, going back at least tens of thousands of years (Beer *et al* 2000).

It is to be expected that the same changes in the global distribution of J_z that accompany the decadal sunspot cycle have been present in past extended solar minima, and will be so in the future, with amplitude proportional to the GCR changes. However, the uncertainty as to how the global upward current I_T varies, due to the responses of the current output of the highly electrified cloud generators to the changes in the GCR flux, precludes any modeling of the J_z changes at this time.

4.2.2. Geomagnetic dipole moment inputs. As discussed in section 2.2.1, GCR particles with magnetic rigidity of about 1 GV/nucleon and higher penetrate unimpeded through the geomagnetic field along field lines within about 30° of the geomagnetic poles. Particles with this rigidity produce ion pairs in the troposphere. At lower geomagnetic latitude (gm-lat) the cut-off rigidity increases, and the GCR flux and thus the ion-pair production rate is reduced. With reductions in the geomagnetic dipole moment, such as occur on century to millennial timescales (Shea and Smart 2004), the gm-lat for a given cut-off rigidity is reduced, so that the polar cap regions of maximum GCR ionization rate expand, and ionization rates equatorwards of about $\pm 60^\circ$ gm-lat are increased.

The effect of this on the global distribution of J_z depends on how much I_T responds to the increase in GCR flux at low latitudes, where most of the deep convection and cloud electrification occurs. As noted earlier, in the first part of the 20th century, when solar activity was lower and GCR fluxes were higher than at present, what little sparse and noisy data exists suggests a decrease in I_T with increasing GCR flux, i.e. the opposite variation to that in the latter half or the 20th century. If this were the case the changes in the gm-lat distribution of J_z could be complex, with decreases polewards of $\pm 60^\circ$ gm-lat on account of the constant R with the decreased I_T and V_i ; and uncertain changes at middle and low latitudes, depending on whether the percentage decreases in R are greater or smaller than the percentage decrease in V_i .

4.2.3. Milankovitch modulated seasonal insolation I_T inputs. The Milankovitch cycles of high latitude increases and decreases in ice cover are well correlated with changes in Earth's orbital parameters, with the 23 000 year cycle due to the effect of precession in shifting the time of perihelion through the seasons in a given hemisphere. Perihelion in winter gives increased insolation with increased temperatures at high latitudes and increased deposition of snow, due to the higher absolute humidity for precipitating storms. The associated aphelion in summer gives cooler temperatures and less melting

and loss of ice, with the combined effect a gradual buildup of the ice sheets. About 11 500 years later with perihelion in summer and aphelion in winter the opposite changes occur, and a loss of ice cover. Changes in the obliquity of the Earth's axis with a 41 000 year cycle produce similar effects. The focus in models of these climate changes has been on the changes in insolation at high latitudes due to these orbital variations (e.g. Ruddiman 2001), but it is also the case that changes in the global circuit with these periodicities will occur independently of the climate changes, as well as a result of them, as follows:

At present there is about 7% more insolation in the tropics at perihelion in January than at aphelion in July. The annual maximum of I_T is in the northern summer with the July/January ratio in the range 10–20% (section 4.1.1), attributed to the preponderance of heating in the northern hemisphere land masses. This is in spite of the 7% weaker insolation, which implies lower mean temperatures, averaged over low latitudes in both hemispheres, in July as compared with January. According to the summary by Williams (2005) a 1°C increase in land surface temperature generates about a 50% increase in lightning on diurnal to semiannual timescales, and about a 20% increase on annual to decadal timescales. Thus the weaker irradiance in July acts in opposition to the 20% effect due to the hemispheric asymmetry. In 11 500 years when perihelion is in the northern summer, the July/January ratio in I_T could be approximately doubled, reflecting a 23 000 year periodicity in V_i and J_z .

Also, the 41 000 year periodicity is likely to be present, on account of the same preponderance of northern hemisphere low latitude land masses. With a more nearly overhead sun for the northern hemisphere maximum in I_T , the magnitude of this maximum is likely to follow the increases and decreases in the obliquity.

A separate effect is a response to changes in the annual mean low-latitude temperatures, which are thought to decrease by as much as 5°C during the ice ages (Ruddiman 2001, p 298). With I_T changing by tens of per cent for a 1°C surface temperature change, there would be a large reduction in mean annual values of V_i and J_z .

5. Observed cloud and meteorological responses to inferred V_i and J_z changes

5.1. Observations of charges on droplets at cloud boundaries

Observations of charges on droplets in weakly electrified clouds are difficult to make, on account of the charging of instrument surfaces by the impacting charged droplets. The problem has been overcome in a new instrument design, which has a counterflowing stream of gas preventing droplets impacting surfaces that are required to be uncharged. The instrument and the results of a flight into stratus clouds over Lake Michigan are described by Beard *et al* (2004). At cloud tops droplets with positive charge in the range $80\text{--}90e$ were found in downdrafts for droplets of radii $6\text{--}8\ \mu\text{m}$. Near cloud base droplets were found with negative charge in the range $50\text{--}70e$, in updrafts. The differing sign of the charges near the two boundaries, and their magnitudes are consistent with the

calculations of droplet charging resulting from the flow of J_z through clouds, discussed in section 2.5.

The results of a large number of measurements on mostly relatively larger cloud droplets are given by Takahashi (1973), as also by Pruppacher and Klett (1997, section 18.4), and the extrapolation of the trend with decreasing droplet size fits the Beard *et al* (2004) results, which on account of the instrumental improvements can be considered reliable. Charges on aerosol particles were not measured, but the charge for a given particle size can be inferred from the droplet charge using the theory of section 2.5. The droplet charges and inferred particle charges are large enough to influence cloud microphysical processes that affect cloud cover and precipitation, as described in section 6.

5.2. Macroscopic cloud and meteorological responses

For many years correlations of meteorological and climate parameters with solar activity and its proxies, on a wide range of timescales, have been reported. The timescales include the multidecadal through millennial range (Eddy 1977, Stuiver *et al* 1995, Ram and Stolz 1999, Hong *et al* 2000, Bond *et al* 2001, Neff *et al* 2001, Wang *et al* 2005), and on these timescales the solar changes are represented by variations in cosmogenic isotopes, while the climate changes are represented by proxies such as oxygen isotope changes in ice cores, the width of tree rings, isotope changes in layered stalactites, and changes in composition in layered ocean and lake sediments.

Correlations of pressure, temperature, precipitation and atmospheric dynamics on the decadal solar cycle using direct atmospheric and sunspot observations have been widely reported in the last two centuries, as described by Herman and Goldberg (1978), van Loon and Labitzke (1988), Brown and John (1979), Venne and Dartt (1990), Hoyt and Schatten (1977), van Loon and Shea (1999), Kodera (2003), Benestad (2002) and Huth *et al* (2007).

The correlations on the day-to-day timescale are the most useful for determining mechanisms, as explanations in terms of changes in solar radiative output (total solar irradiance and UV irradiance) can be ruled out when the meteorological parameters are found to correlate with the arrival at the Earth of solar wind disturbances caused by solar activity. (There is an average of four days propagation time for the solar wind disturbances from Sun to Earth, as compared with 8 min for the radiative changes.) On the decadal and longer timescales both the radiative and solar wind-modulated inputs, including GCR, show similar variability, and thus from correlations there is ambiguity as to whether radiative or solar wind changes are responsible. Because of this ambiguity, and because this review is concerned with atmospheric electricity and the global circuit, we do not consider radiative effects further. Also, with tens to hundreds of events to analyze on the day-to-day timescale, the background noise, which is usually of comparable magnitude to the responses, can be averaged out in the analysis, and the statistical significance of the correlations can be determined.

Observations showing day-to-day cloud and meteorological responses to J_z have been reviewed by Tinsley *et al* (2007).

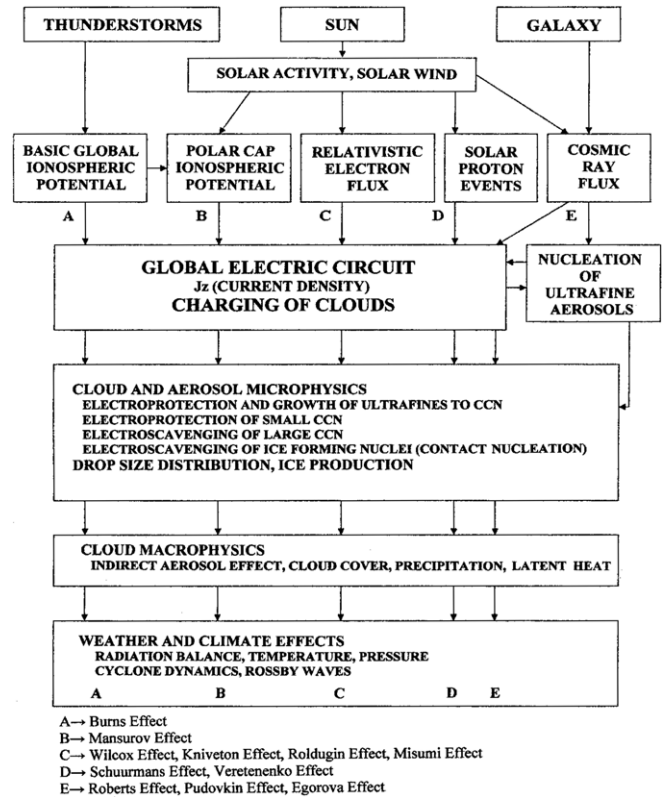


Figure 7. Connections between weather and climate with thunderstorms, solar activity, and galactic cosmic ray flux, via the global atmospheric electric circuit and cloud and aerosol microphysics. The five independent forcing agents (A through E) all affect the ionosphere-earth current density J_z . Day-to-day meteorological responses correlate independently with each of these inputs, and are named at the bottom of the flowchart, and are described, with references, in the text and in appendix A. The hypothesized cloud microphysical and macroscopic processes that connect J_z and the meteorological responses are indicated in the fifth and sixth row of boxes, and are discussed later in the text.

Figure 7 is a flow chart from that paper that illustrates the associations between the four external inputs and one internal input to the global circuit (labeled A to D) that affect J_z (as described in sections 2–4) and the atmospheric responses that correlate with them. There are two ways of classifying these observed correlations. First we will consider them in terms of the five inputs as in figure 7, and then in terms of two different pathways for macroscopic atmospheric effects, with each pathway associated with one or more of the five inputs.

5.2.1. Classification by input to the global circuit. Each of the five inputs, i.e. one internal (A) input and four external (B, C, D and E) inputs, as represented in the third row of boxes in the flow chart, is associated with one of the sets of meteorological ‘effects’ listed as A to E below the flow chart. They are summarized, with references, in appendix A. In each case the correlations are found in onset time, duration, sign and amplitude with the particular forcing agent. We now consider each set in turn.

The response to the basic ionospheric potential (input A, which changes J_z on the day-to-day timescale as described in section 4.1.2) has been analyzed so far only for surface

pressure in polar regions (Burns *et al* 2007, 2008). The Burns effect consists of correlations of daily average surface pressure, measured at various locations, with the daily average of PG values, measured so far only at Vostok, Antarctica. The Vostok PG values are corrected to remove the small solar wind effect, and the correlation has been observed in 1998–2001 data with high statistical significance for seven stations in the Arctic and eleven stations in the Antarctic.

The responses to the solar-wind-induced day-to-day changes in polar cap ionospheric potential (input B, described in sections 2.1.2 and 4.1.3 and figure 2) were first analyzed in 1964 IQSY data by Mansurov *et al* (1974), as differences between daily average surface pressure values for ‘towards’ as compared with ‘away’ solar wind sectors. The pressure changes, ΔP , are of amplitude a few hPa, and are opposite in the Arctic as compared with the Antarctic, consistent with the opposite V_i and J_z changes in those regions with sector changes. A new analysis for 1995–2005 data by Burns *et al* (2007, 2008) was made with respect to the IMF B_y component, and showed the effect with high statistical significance. The B_y changes, ΔB_y , showed persistence corresponding to periodicities of approximately 27 days, and the amplitude can be converted to an ionospheric potential change, ΔV_i , using one of the Weimer (1996, 2001) models. For comparison, the measured PG changes in the Burns effect had a persistence of 4 or 5 days, and can be converted to ΔV_i changes by scaling the mean PG value on the mean ionospheric potential (near 250 kV). When these conversions to ΔV_i are made the ΔP changes in both the internal Burns effect and the smaller but longer persisting external Mansurov effect are found to have the same $\Delta P/\Delta V_i$ ratio within experimental errors. This is consistent with J_z as the link to the atmospheric response, with equivalent effects for either internal or external forcing.

The responses to reductions of relativistic electron precipitation (input C, described in section 2.2.3) were first observed as a reduction at HCS crossings of the areas of high vorticity of northern hemisphere winter storms by Wilcox *et al* (1973), and were subsequently confirmed with new crossings by Hines and Halevy (1977), and with an especially sensitive analysis by Larsen and Kelly (1977). Kirkland *et al* (1996) related the decreases in areas of high vorticity to relativistic electron flux decreases at HCS crossings at times of high stratospheric aerosol loading. As discussed in section 2.2.3, the flux decreases produce J_z decreases at mid-high latitudes, when there is a high concentration of aerosols in the stratosphere. The negative results for responses to HCS crossings found by Williams and Gerety (1978) were for periods of low stratospheric aerosol loading, and are consistent with the need for both stratospheric aerosols and J_z changes as essential links in the phenomenon. Other responses to input C are those of changes in cloud cover (Kniveton and Tinsley 2004) for the Pinatubo stratospheric volcanic era; changes in atmospheric transmission (Roldugin and Tinsley 2004) for the El Chicon volcanic era; and changes in 500 hPa temperature (Misumi 1983) for the Agung volcanic era. For each of these eras, winter vorticity decreases associated with relativistic electron flux changes or HCS crossings were found (Kirkland *et al* 1996).

The responses to solar proton events (input D, section 2.2.4) that are associated with J_z increases at high latitudes have been found in terms of pressure increases at 500 hPa centered on the north magnetic pole by Schuurmans (1965), and vorticity increases near Greenland by Veretenenko and Thejll (2004, 2005). The pressure and vorticity increases were for about a day. The vorticity increase with the J_z increase makes a consistent pattern with the vorticity decreases associated with the J_z decreases of the Wilcox effect.

The responses to decreases in GCR flux (Forbush decreases; input E, in section 2.2.1) were the first day-to-day response to be discovered, and were first apparent as correlations of surface pressure in winter storms with magnetic storms, since data on these were available since the beginning of the 20th century (see Duell and Duell (1948), Macdonald and Roberts (1960) and their references to earlier work). Objections that magnetic storm signatures might be influenced by winter storms led to the suggestion that HCS crossings be used as totally independent markers for solar wind changes (Markson 1971). Also, responses of winter storm intensity were made more objective by being characterized by the vorticity-area index or VAI (Roberts and Olson 1973), which led to the discovery of the stronger Wilcox effect (Wilcox *et al* 1973), but this unfortunately distracted attention from the more reliable correlations with magnetic activity, which in turn generated skepticism about the reality of all Sun–weather effects when the Wilcox effect disappeared (Williams and Gerety 1978). Time series of the VAI were published (Olson *et al* 1977, 1979) and enabled Padgoankar and Arora (1981) to re-examine the winter VAI response to magnetic storms. They found that the VAI response persisted in eras when the Wilcox effect at HCS crossings was not present. Magnetic storms usually follow solar flares and are usually accompanied by Forbush decreases, and work by Tinsley *et al* (1989) and Tinsley and Deen (1991) showed that the clearest VAI response for winter storms was that associated with Forbush decreases. These produce J_z decreases at middle and high latitudes by changes in tropospheric ionization, and thus the J_z change is independent of stratospheric aerosols. We now call this association the Roberts effect, and it is another example of the consistent pattern of vorticity responses to J_z changes. The VAI time series has been updated by Thejll (2002). Other responses to Forbush decreases (input E) have been observed at high latitudes in the form of changes in high altitude cloud cover (Pudovkin and Veretenenko 1995, Todd and Kniveton 2001) and changes in atmospheric temperature and pressure (Egorova *et al* 2000).

Responses to input D followed by input E were evidently observed as pressure changes by Schuurmans and Oort (1969) and as VAI changes by Olson *et al* (1975). A combination of input B and input C was evidently observed by Rostoker and Sharma (1980) as surface pressure changes.

5.2.2. Classification by pathway for amplification. As noted by Tinsley and Deen (1991) there is evidently an amplification of energy from the GCR input (or the global circuit changes, which have about the same energy) to some of the meteorological dynamical outputs by a factor of order 10^7 .

For an acceptable mechanistic explanation this amplification should be accounted for. All the short term responses can be related to electrically altered scavenging processes in clouds, as represented by the several processes listed in the box on the fifth row in figure 7 and discussed in section 6. It appears that when large amplification follows these, it can be by at least two different additional mechanisms, in different cloud environments, as listed in the boxes in the sixth and seventh rows of figure 7.

Amplification in winter storms. One environment with available energy appears to be in baroclinic instabilities in pressure and temperature in the winter general circulation. In this environment the vorticity changes (the independent Wilcox, Veretenenko and Roberts effects for inputs C, D, and E) are consistent with a scenario outlined by Tinsley *et al* (1994) in which changes in J_z create changes in space charge at the boundaries of layer clouds, resulting in changes in ice production via contact ice nucleation, due to electrically enhanced changes in the scavenging of contact ice nuclei. The layer clouds associated with the warm front in winter cyclones are an attractive location for initiation of the amplification, as they are wedged upwards as the front progresses, and as the cloud top temperatures fall through the 0° to -15° range contact ice nucleation occurs at warmer temperatures and thus earlier than other ice nucleation processes (Tinsley *et al* 2001). The supercooled droplets freeze and then grow rapidly by the Wegener–Bergeron–Findeisen process (Tinsley and Deen 1991) and enhance the precipitation from clouds at lower levels by the seeder–feeder process (Rutledge and Hobbs 1983). For an increase in J_z the net result is an increase in precipitation and an increase in latent heat released into the storm, with enhanced updrafts, and an increase in storm vorticity (Posselt and Martin 2004, Lapeyre and Held 2004). Thus momentum from the baroclinic winter circulation is dissipated into eddies and surface friction. With active eddy-mean flow interaction, and ‘positive feedback between storm track anomalies and more slowly varying flow’ (Chang *et al* 2002) there is a possibility that decadal variations in ‘storm track intensity’ (Chang and Fu 2002) may play a role in the decadal solar cycle variations of mean flow described in section 5.2. It is a reflection on the inadequacy of present cloud models, which among other simplifications do not include electrical effects, that current forecasting models are ‘nudged’ into better agreement with actual storm dynamics by real-time radar measurements of precipitation rates, that are translated into latent heat release rates and their effects on storm dynamics for subsequent forecasts (Jones and Macpherson 1997). Another role in both the day-to-day vorticity variations and decadal storm track variations may be played by cloud cover variations due to J_z variations, as reviewed in the next section.

The response of winter storm vorticity to J_z has been observed for responses to inputs C, D, and E, and since one J_z input is equivalent to another, vorticity responses to all sources of J_z variability (at the latitudes of cyclogenesis) are to be expected, and for the southern as well as the northern hemisphere. One can predict that vorticity correlations with input A will be found when long and accurate enough time

series representing day-to-day V_i and J_z changes from the internal generators become available. As with the Burns effect, this could be considered an ‘electrical teleconnection’ between meteorology in the low-latitude generator regions and the meteorology at higher latitudes.

Radiative effects with layer clouds. Another sensitive environment appears to involve layer clouds, and especially thin layer clouds, where latent heat effects are not important. Here the cloud cover or cloud thickness or cloud lifetime changes can result in energy amplification via changes in the amounts of incoming shortwave solar radiation and outgoing longwave thermal radiation, with consequences for tropospheric heating and cooling that cause changes in surface pressure and atmospheric dynamics. Dickinson (1975) noted that a change in upper level cloud opacity by 20% would produce heating rates in the column below of the order of 0.1°C per day, which as a differential across a zone 15° in latitude would lead to changes in zonal winds at the tropopause of the order of 2 m s^{-1} . Such situations apply to cloud cover changes in the Pudovkin effect and the Todd effect (input E) and the Kniveton effect and the Roldugin effect (input C).

Given that the inputs C, D and E contain latitude gradients and extend over the cyclogenesis regions, an alternative explanation for vorticity changes (Veretenenko and Thejll 2004, 2005) is that latitude-dependent gradients in cloud cover and radiative effects appear across the polar fronts, changing the baroclinic gradients and thus the resulting cyclone vorticity. It should be possible to investigate the relative contributions from both the latent heat mechanism and the radiative mechanism with suitable adjustments to cloud cover and precipitation efficiency in winter cyclone models, and then investigate longer term effects on Rossby wave amplitude and the general circulation.

The Egorova effect (input E) polar cap pressure response appears to be the result of the Todd effect (input E) on high cloud cover response in Antarctica. The changes in the polar cap atmospheric pressure in the Burns effect (input A); the Mansurov effect (input B); the Schuurmans effect (input D) and Egorova effect (input E) suggest that the polar atmospheres are additional environments where cloud responses can be further amplified. It is possible that radiative balance changes affect unstable katabatic wind regimes in Greenland and especially in Antarctica (Troshichev and Janzhura 2004) and the coupled polar vortex (Parish and Bromwich 1991). Polar vortex strength changes can produce the observed pressure changes. Because J_z variation from one source is equivalent to that of another, one can predict that cloud cover changes will be found over Antarctica correlated with the other inputs that vary in that region, i.e. with inputs A, B and D to explain the Burns, Mansurov and Schuurmans pressure effects.

It is evident that the responses to inputs A, B, C and D are not via ion-induced nucleation (section 2.4.2) affecting clouds, as there is no significant change in tropospheric ionization associated with these inputs. However, it is not clear which of the several microphysical processes listed in the box in the fifth row of figure 7 would be more effective for layer cloud changes. One possibility involves electroscavenging of large

and giant CCN, while at the same time the electroprotection of the smallest CCN against phoretic and Brownian scavenging, that leads to a narrowing of the CCN size distribution and an increase in concentration of the smallest CCN. The result is the ‘indirect’ aerosol effect, or Twomey effect, with the available cloud water divided among a higher concentration of droplets of smaller average size and narrower size distribution. This reduces the coagulation and precipitation rates, increases cloud lifetime, cloud cover and albedo, and changes the radiative balance of the atmosphere. The microphysical processes will be reviewed in section 6.

The GCR variations (input E) produce tropospheric ionization changes, but also J_z changes, and the atmospheric responses to input E are of the same type and comparable amplitude for a given J_z change as those for inputs A through D. Thus a mechanism involving J_z is necessary (for inputs A through D) and sufficient (for A through E), whereas solar irradiance mechanisms and ion-mediated nucleation are neither necessary nor sufficient for the whole set. This is not to rule out ion-mediated nucleation as being important in other ways for climate change. But J_z /cloud processes are clearly necessary for the day-to-day timescale. The J_z /cloud processes are applicable to the longer time scales, and it has not yet been demonstrated that the irradiance and ion-mediated nucleation mechanisms are required for the longer term climate changes that correlate with solar activity.

5.2.3. Decadal cloud cover and precipitation. On the decadal solar cycle timescale Kniveton and Todd (2001) found increases in precipitation efficiency at high latitudes with increases in the GCR, which are inconsistent with the ion-mediated nucleation process that decrease precipitation, but consistent with increased contact ice nucleation with increasing J_z . Satellite observations of decadal global cloud cover changes that correlate with the GCR flux (Svensmark and Friis-Christensen 1997) have been identified as due to low level clouds (Marsh and Svensmark 2000). Ion mediated nucleation has been invoked to explain these results, as also those of Harrison and Stephenson (2006). Svensmark *et al* (2007) have recently made laboratory measurements of the process of ion-mediated nucleation and found that nucleation rates of particles of at least 3 nm diameter were proportional to the negative ion concentration. Much more work is required on the mechanism of growth, with non-water volatiles, to CCN size (~ 50 nm diameter, which is an increase in mass by $\sim 10^4$), and to show that the resulting production rate of CCN can be competitive with CCN production by other processes. As noted in previous sections, all the correlations that have been attributed to variations in ion-mediated nucleation, as well as to irradiance effects, can be understood as due to J_z effects.

Ground based observations of decadal changes in cloud cover and solar insolation have been analyzed by Veretenenko and Pudovkin (1997, 1999, 2000), and Udelhofen and Cess (2001), with mid-latitude continental observations showing the opposite correlation with the solar cycle to those of Marsh and Svensmark (2000) for mostly oceanic clouds. Usoskin *et al* (2006) have reanalyzed decadal satellite cloud cover data showing regional differences in correlations involving

both high and low clouds. As noted in section 5.2 there are very many reports of correlations of atmospheric dynamics and other meteorological parameters with the decadal sunspot cycle. Therefore, as modeled by Takemura *et al* (2007), there is a possibility that on decadal timescales the dynamical response of the atmosphere to an initial cloud cover changes itself produces additional changes in cloud cover and precipitation, thus obscuring the location and sign of the initial effect. With regard to differing responses for continental versus oceanic clouds, the differing aerosol concentrations and the differing rates of occurrence of deep, highly electrified convective clouds is likely to be important.

The possible pathways connecting J_z with microscopic and macroscopic meteorological changes, as indicated in the boxes in the fifth and sixth rows of figure 7, will now be reviewed.

6. Theory for electrical effects of charge on scavenging

The microphysical scavenging of aerosol particles by water droplets in clouds has important effects on the macroscopic cloud properties, which affect atmospheric temperature and dynamics. Electrical charge on the aerosol particles and droplets changes the scavenging rates, either by increasing the scavenging rates ‘electroscavenging’ or decreasing the scavenging rates ‘electroprotection’ that would otherwise occur due to other scavenging processes. The main charging process for clouds with weak electrification (normally in the absence of ice) and especially for layer clouds, is from the production of space charge in the conductivity gradients at cloud boundaries, as described in sections 2.5 and 5.1. The charges on droplets are larger, on account of their larger radii, than the charges on particles. However, highly charged particles can be produced by the evaporation of charged droplets (Beard 1992) with the lifetime of the high charge on the particles of 15 min or so (Tinsley *et al* 2000), which is long enough to affect scavenging rates.

There are several effects to be considered, arising from scavenging of cloud condensation nuclei (CCN) and ice-forming nuclei (IFN) by droplets (in the latter case most importantly by supercooled droplets that then freeze by contact ice nucleation and initiate precipitation) and the scavenging of CCN and IFN by ice in ice clouds. Scavenging and processing of background aerosol are also enhanced.

6.1. Calculating the electrical force

Depending on the sizes and charges on the aerosol particles and the droplets or ice crystals there is an electrical force between them. For simplicity we may refer to any or all these three entities as ‘objects’. The electrical force is present when only one object of a pair is charged, but generally there would be charges on both. In earlier simulations of the effect of these forces on cloud microphysics only unlike charges were considered (as reviewed in the book by Pruppacher and Klett 1997). However, intermingling of objects with unlike charges is a much less common situation than the intermingling of them with like charges, as in space charge layers at cloud boundaries.

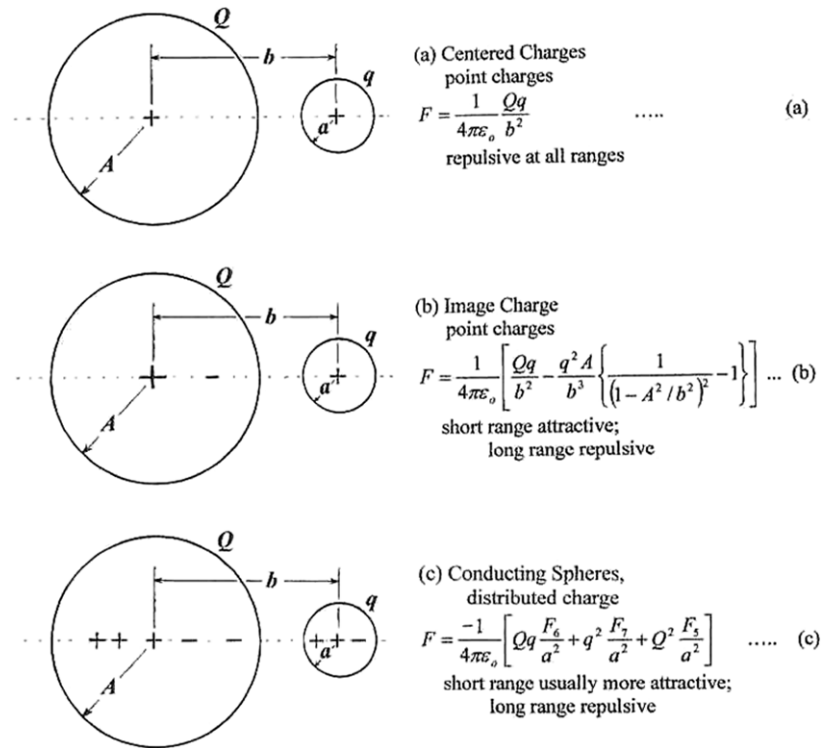


Figure 8. Three treatments that have been used to calculate the electrical force between charged spherical conducting objects, such as between water droplets, or between a droplet and an aerosol particle. The simplest (a) is the Coulomb force between charges centered in the objects; an improvement (b) that applies to a small object near a larger one includes a point image charge on the larger one; while the exact treatment (c) for spherical conducting objects of all size ratios treats distributed charges on them.

It was shown by Tinsley *et al* (2000) that when pairs of objects of different sizes have the same sign charges there can be an increase in collision efficiency compared with the case of them being uncharged. There is a long-range electrical repulsive force between objects with the same sign charge, but a short-range attractive force due to the production of image charges. Smaller charged objects can be carried by the flow of air close enough to a faster falling larger object, against the long-range repulsive force, for the short-range attractive force to predominate, and ensure collision. Figure 8 illustrates two spherical objects of radii A and a and with charges Q and q on them, with spacing of centers b . For Q and q of like sign, and when only centered charges are considered, there is only the repulsive Coulomb force (expression (a) in figure 8). Figure 8(b) shows a single image charge induced only on the large spherical object by the charge on the smaller one. The second term on the right of expression (b) in figure 8 is due to the image charge, which becomes strongly attractive as the spacing between surfaces $s = b - (A + a)$ becomes small compared with A . If $q = Q$ the crossover from long-range repulsion to short-range attraction is at $b/A = 1.6$. Expression (b) becomes exact for $a/A \rightarrow 0$.

For a not negligible with respect to A the exact treatment of the electric force that is applicable to finite spherical conducting objects in the absence of an external ambient polarizing electric field is given in figure 8(c), where the charges are distributed (axisymmetrically) in the two objects, and the electrical force is given by expression (c) in figure 8.

The conductivity of water droplets is sufficiently high so that charge redistribution occurs in times short compared with the interaction times, so that the treatment as ideal conducting spheres is appropriate (Davis 1969). For aerosol particles that may be poor conductors, lacking salts or acids, their dielectric properties makes the conducting spheres treatment a good representation, unless their dielectric constant is much smaller than that of water (Hall and Beard 1975).

The functions F_5 , F_6 and F_7 in equation (c) of figure 8 are complex polynomial expressions given by Davis (1964a, 1964b) which depend only on the ratio of the radii of the two spheres and their spacing s . The functions F_5 and F_7 are equal for $A = a$. The equation (b) in figure 8 is a good approximation for the ratio A/a greater than about 20, except for s small compared with a . Also, for very large charge ratios Q/q , the dipole induced on the object with little or no charge makes an important contribution to the force. When giant ($a > 1 \mu\text{m}$) aerosol particles are present, with radii a comparable to the droplet radii A , the exact expression (c) gives significantly greater attractive forces for typical charge ratios and A/a less than 20, compared with the image force result. This expression was used by Grover and Beard (1975) and Grover *et al* (1977) for calculating electrical forces between two charged droplets.

Expressions (a), (b) and (c) are also valid for opposite signs of Q and q , where the attractive forces are considerably stronger. For situations where an ambient electric field in a cloud is very strong, as in deep convective storms, Davis (1964a, 1964b) has given additional polynomial terms for

evaluation of the force between the two spherical objects, due to the interaction of the induced dipoles on them, and these were used by Schlamp *et al* (1976, 1979) for interactions between two charged droplets in strong electric fields.

6.2. Calculating the trajectories and collision efficiencies

The electrical force between two charged objects in air, such as spherical droplets and aerosol particles, is one of several forces that determine the trajectory of one object relative to the other. A vector force equation that has been used in previous treatments of scavenging when inertia was important (e.g. Grover and Beard 1975) can be applied separately to each object, and generalized slightly to become:

$$m(dv/dt) = mg^* + (v - u)/B_p + F, \quad (27)$$

where m is the mass of the object; v is its velocity in an inertial reference frame; g^* is the net acceleration of gravity taking into account the buoyant force of the air; and the second term on the right is the Stokes–Cunningham drag on the object where u is the velocity of the air and B_p is the mobility of the object. F represents the sum of the radial forces, which are the electrical force F_e , the thermophoretic force F_{Th} , and the diffusophoretic force F_{Df} . These two phoretic forces are associated with evaporation, if one or both of the two objects involved is a water droplet and the humidity is below 100%. The parameters v , u , g^* and F are vector quantities, and the detailed expressions for the phoretic forces, mobility etc, together with the values of the relative constants, are given by Tinsley *et al* (2006, appendix A), based on the extensive work in this field reviewed by Pruppacher and Klett (1997) and Young (1993).

The calculation of collision efficiencies between droplets and aerosol particles is relatively fast and uncomplicated for typical cloud droplets and aerosol particles with a/A smaller than about 0.05, in which case the droplet can be considered falling vertically and unaffected by the interaction with the particle, the particle inertia can be neglected and the image electrical force can be used. The collision efficiency E_C can be defined as the fraction of the volume swept out by a droplet (larger object) as it falls, to that containing the centers of the particles (smaller objects) that it collides with. This amounts to a scaling factor on πA^2 to give the cross section of the droplet for collision with particles. An alternative definition for larger particles expands the radius of the cylindrical volume swept out by the droplet by adding to it the radius of the particles, with E_C smaller by a factor $A^2/(A+a)^2$.

The trajectory calculations of Tinsley *et al* (2000) for small aerosol particles neglected their mass and phoretic forces, which greatly simplifies equation (27). The air stream was considered to be moving upwards with the velocity U_∞ relative to the droplet, where U_∞ is the terminal velocity of the droplet, and the origin of coordinates was the center of the droplet. At the location (r, θ) of the particle the velocity u of the air was given by expressions for Stokes flow with stream velocity U_∞ . The expression for the electrical force

was that for the single image charge. Starting from a distance $6A$ below the droplet, particle trajectories were numerically calculated to determine the initial offset, relative to the vertical axis through the droplet center, of the trajectory that just intersected the droplet surface. The ratio of this offset to A was designated x_{max} , and the collision efficiency was then $E_C = (x_{max})^2$. Without charge, and for particles of radius 10^{-2} to $1 \mu\text{m}$, typical values of E_C in the absence of phoretic forces are $E_C \sim 10^{-2}$ – 10^{-3} . This is because the laminar flow carries the small particles around the droplet so that they do not collide with it.

The results of the trajectory calculations showed that with quite small charges on the particles, such as charges resulting from evaporation of charged droplets, or as in the space charge layers at cloud boundaries, the collision efficiencies could be considerably enhanced. The enhancement was sufficient to suggest that even in weakly electrified clouds, the electrical effects make a significant contribution to scavenging rates for IFN and CCN. Another result was that the process of scavenging of charged particles of like sign can significantly increase the charge on the droplets.

The very small aerosol particles have very high mobility, such that the long-range electrical repulsive force can keep them out of range of the short-range attractive electrical force, and also keep them far enough from the droplet that scavenging by phoretic forces and Brownian diffusion is inhibited. This is the electroprotection process, as noted earlier, and it applies to particles of radii below about $0.1 \mu\text{m}$ for typical droplet radii and charges in weakly electrified clouds.

For trajectories of particles of radii greater than $1 \mu\text{m}$ the inertia of the particles becomes important, and the full equation (27) must be solved as a second order differential equation for numerical integration along the trajectory, as in Tinsley *et al* (2006). This work also utilizes flow fields that take into account the non-Stokes asymmetries of the flow in the upstream and downstream regions, and the effect of the flow around the particle in modifying the otherwise vertical trajectory at constant speed of the falling droplet. The trajectories of both the particle and droplet were determined by applying equation (27) to each, and calculating increments to first one and then the other object, starting with the particle a distance $12A$ below the droplet.

Figure 9 shows examples of the results for collision efficiency, to illustrate some of the complexities of the variations found. These results are from Tinsley *et al* (2006), where the image charge electrical force was used. These results are in the absence of phoretic forces (100% humidity). The spherical particles are of radii from 0.1 to $10 \mu\text{m}$, being scavenged by droplets of radius 15 to $40 \mu\text{m}$. The charge on the droplet is $100e$ in all cases, and two values of particle charge are used, $20e$ and $200e$. The families of curves are for densities ranging from 2500 to 300 kg m^{-3} , or specific gravity (SG) from 2.5 to 0.3 as labeled. The results for the lowest densities can be used as an approximation for the electroscavenging of giant nuclei. These may be formed as loose aggregates of coagulated aerosol particles, possibly after scavenging by droplets that then evaporate. A correction is required to account for the non sphericity of the particle for electric and drag forces. The

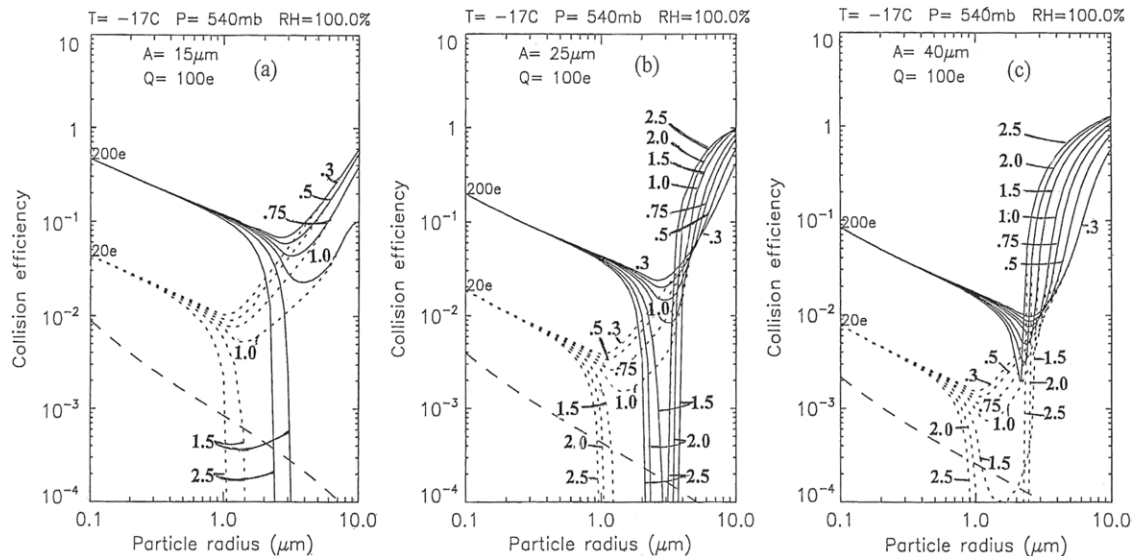


Figure 9. Effects of particle specific gravity and electrical charge on collision efficiencies for particles, as a function of radius a from 0.1 to 10 μm , being scavenged by droplets of radii (A) 15 μm , (b) 25 μm , (c) 40 μm . The droplets all have charge 100 e , with the solid curves for particle charge 200 e , and the dotted curves for particle charge 20 e . The particle specific gravities range from 2.5 to 0.3 as labeled. The curves with large dashes are for the collision efficiency due to Brownian diffusion.

temperature and pressure were for mid-tropospheric levels. The collision efficiency due to Brownian motion is shown as the large dashed curve in each case.

For particles of radii less than about 1 μm , the electrical force is dominant and effects of weight and inertia become insignificant. For particles between about 1 and 3 μm , with SG about 1 or greater and only 20 e of charge, the weight of the particles exceeded the electrical attractive force in the stagnation flow region below the droplet, and the particles did not collide ($E_C = 0$), but were swept around the droplet. This regime of low or zero E_C , extending down to a particle radius of about 10⁻² μm in the absence of electrical or phoretic forces, is known as the ‘Greenfield gap’ and the effect of increasing charge is to increasingly narrow or even close it. The Greenfield gap is bounded on the large particle side by the rise in collection efficiency due to inertia, which increases with particle mass as the cube of the radius. The inertial effect also increases with droplet mass, which determines droplet fall speed, and the time available for the flow to drag the particle out of the droplet path. For the 15 μm radius droplet with its relatively slow fall speed, the inertial effects are negligible, and for particles of SG of 1 or less, and radii greater than 1 or 2 μm , the collision efficiency is determined mainly by the ‘interception effect’. This effect is due to the increasing extension across streamlines of particles of increasing radius, with a small effect of weight for the higher values of SG.

A comparison of panels (a), (b) and (c) in figure 9 shows that in the electrical and Greenfield regimes E_C decreases with increasing droplet size. This is because with greater droplet fall speeds there is less time for the electrical forces to act. But in the inertial regime E_C increases with increasing droplet size, to about unity for the highest values of particle SG. (If E_C is calculated as $E_C = x_{\text{max}}^2 A^2 / (A + a)^2$ then the asymptotic value of E_C in the inertial regime is 1.0). Similar

calculations have been made by Tripathi *et al* (2006) for a more restricted range of parameters, using the electrical image force. They have parametrized their results as a function of particle radius, particle density, particle charge and droplet radius.

6.3. Calculating the scavenging rates

For microphysical processes associated with particle scavenging, such as contact ice nucleation and removal of aerosol particles, what is more useful than the collision efficiency is the scavenging rate coefficient, in which the collision efficiency is multiplied by the droplet cross sectional area and the velocity with which it overtakes the particle. The rapidly increasing fall speeds and cross sectional area with increasing droplet radius ensures that the scavenging rate coefficients increase with A , even while collection efficiencies are decreasing (Grover and Beard 1975). Then the scavenging rate coefficient, R , is multiplied by the concentrations of the droplets and the aerosol particles, with a summation over the size distribution of each, to obtain the scavenging rate S_R per unit volume. For monodisperse droplet and particle and charge distributions, with concentration n_A and charge Q for the droplets, and concentrations n_a and charge q for the particles, the value of S_R is given by

$$S_R = R(A, a, Q, q) n_A n_a$$

$$= \pi A^2 (U_{\infty, A} - U_{\infty, a}) E_C(A, a, Q, q) n_A n_a, \quad (28)$$

where $U_{\infty, a}$ is the fall speed of the particle. For polydisperse distributions an integration over the generalized form of (28) is required.

Plots of R as a function of A in the range 5 to 30 μm for values of a from 0.1 to 1 μm are given by Tinsley *et al* (2001) for particles of SG 2.0, with relative humidity 98%

and neglecting inertia. The values of Q ranged from $500e$ to $-100e$, with q values of $50e$ and $20e$. There is a rapid increase in R for the larger droplet sizes. Estimates of the rates of electroscavenging of IFN by supercooled water droplets were made which showed that for temperatures between -15°C and 0°C the rate of contact ice nucleation could be comparable to deposition nucleation, suggesting significant influences of electroscavenging on the production of precipitation in cold clouds. Data from Hobbs and Ragnó (1985) showed that clouds with drop size distributions extending above $a = 10\ \mu\text{m}$ have greatly increased ice concentrations compared with others with distributions not extending that far. This suggests that scavenging processes leading to contact ice nucleation are involved, and since the rates of scavenging in the absence of electrical charge on the IFN were too low to account for the production of ice, it was suggested by Tinsley *et al* (2001) that electrical enhancement of the scavenging was responsible. Similar conclusions were reached by Tripathi and Harrison (2002) on the basis of similar trajectory calculations. However, uncertainties concerning the concentrations and charge distributions on aerosol particles effective as contact ice nuclei prevent robust calculations of contact ice nucleation rates to be made at present, especially under conditions where charged droplets are evaporating and producing relatively highly charged residues that are likely to be efficient as ice-forming nuclei (Beard 1992).

7. Summary and needs for further work

7.1. Progress to date

The basic Wilsonian concept of the global circuit driven by thunderstorms supplying charge to an equipotential ionosphere has been amply verified by modeling and by observations over the globe. These show the same time variations of potential gradient in the universal time diurnal variations; for variations from day to day; for seasonal variability; and for interannual variability; when local noise is taken into account. The Wilson model has been extended by the recognition that highly electrified clouds that are not producing lightning, and shower clouds also contribute to the conduction current that charges the ionosphere. It has also been extended by the inclusion in the circuit of generators in the ionosphere that respond to solar activity. Temporal and latitudinal variations in the distribution of column resistance in the global circuit, due to galactic cosmic rays and other incoming energetic particle fluxes responding to solar activity, have been added to the basic model and confirmed by observations, as also have been the effects of variations of aerosol populations in the troposphere and stratosphere. Long term changes in the circuit parameters due to climate change in the generator regions; to orbital, solar activity and GCR variations; and to geomagnetic dipole moment changes are predicted.

Observational evidence is clear for effects of the ionosphere-earth current density J_z on clouds, affecting precipitation, atmospheric temperature and dynamics. Modeling suggests that the mechanisms include electrical effects on scavenging of ice-forming nuclei and condensation nuclei,

with possible contributions from ion-induced nucleation. But details of the mechanisms remain unclear. The observed responses are due to changes of order 10% in J_z and GCR flux, and are thus second order effects. The first order effects are evidently part of basic aerosol-droplet processes in clouds.

A picture is emerging in which different types of clouds respond in different ways to both internally and externally forced changes in atmospheric electricity. Then, in certain types of environment (e.g. winter cyclones, layer clouds) there is a potential for further amplification of the electrical input (e.g. by latent heat transfer, or changes in radiative balance) to produce dynamical changes, affecting atmospheric circulation. New responses are predicted for short term and long term global circuit changes. Much work remains to be done to investigate these electrical effects on clouds, and to provide complete quantitative accounts of them.

7.2. Needed further work

7.2.1. Global circuit observations and models. There is uncertainty as to how the global tropospheric generator output I_T responds to changes in cosmic ray flux, and to climate cycles, such as the El Niño-Southern Oscillation, the Pacific Decadal Oscillation, the North Atlantic Oscillation, etc. This uncertainty can be resolved from observations of J_z and E_z , preferably with σ_1 and σ_2 measurements to provide an Ohm's Law check, from clean, low humidity, low turbulence, high altitude sites, such as the Antarctic and Greenland ice plateaux, the Tibetan plateau or the Andes and oceanic and continental mountain sites that are high and minimally affected by aerosol and humidity. The observations should be continued for at least several decades, to separate the solar cycle and climate cycle effects. Simultaneous observations from several sites in opposite hemispheres are needed to determine the global variations, by separating out local conductivity variations and averaging meteorological noise.

With day-to-day global variations evaluated to 1% or better, the relationship to observed and predicted meteorological and GCR variations in the generator regions can be determined. Also, global and regional cloud cover and dynamical responses to the global circuit variations can be evaluated, and predictions of expected correlations can be tested. Ultimately it may be possible, by forecasting changes in the internal and external generator regions, including inputs from the sun, to forecast the contribution of the global circuit to global weather and climate.

It is desirable to use atmospheric models to relate changes in both precipitation efficiency and in the latitudinal gradients of cloud cover to vorticity changes in winter cyclones. Since areas of high vorticity rapidly dissipate momentum from the general circulation, the effects on zonal wind speed and Rossby wave amplitude should be evaluated. Integrated seasonal and decadal changes could then be compared with changes in atmospheric dynamics that correlate with the solar cycle (section 5.2).

There is a need for improvement in global circuit models, particularly for the inclusion of clouds and ultrafine aerosol

layers in column resistance calculations. Models of the generator clouds could help clarify the response of I_T to changes in GCR flux. For understanding long term climate change, models of changes in I_T production during periods of colder or warmer low-latitude temperatures would be useful. Also, global circuit models for periods of reduced geomagnetic dipole moment, with the very different global distributions of conductivity, are needed for understanding effects on climate in past and future large geomagnetic field excursions.

7.2.2. Laboratory work. Laboratory work in cloud chambers with capabilities for producing atmospheric ions is needed to test the effect of ionization on nucleation mechanisms, and to test the models of electroscavenging and electroprotection, with charges and sizes of droplets and aerosol particles in the ranges found in weakly electrified clouds.

7.2.3. Microphysical parametrization. Further microphysical parametrization is required to derive collision rate coefficients in a form suitable for use in mesoscale and global circulation models. A formalism that combines electrical effects on scavenging with phoretic and Brownian scavenging is needed to include the reduction of the latter two by electroprotection for the smaller CCN.

7.2.4. Charges in clouds. There is a need to measure the charges on droplets and aerosol particles at cloud boundaries in a much more comprehensive way than has been done so far. While aircraft give horizontal profiles through different cloud regions, vertical profiles from probes suspended below balloons that are descending or rising are needed. The simultaneous measurement of aerosol particles (especially CCN and IFN) size distributions, and droplet and ice particle size distributions are needed, with observations during all stages of cloud formation and dissipation, as well as in downdrafts and updrafts. Then, modeling of the observational conditions should follow, to test and quantify the physics of the cloud models.

Acknowledgments

This work has been supported by the US National Science Foundation grant ATM0242827 to the University of Texas at Dallas.

Appendix A. Summary of day-to-day meteorological effects correlating with J_z

Input A: Global ionospheric potential

A1: Burns effect. Correlation of surface pressure with global ionospheric potential with persistence 4–5 days, and amplitude 3–5 hPa. Observed for seven stations in the Arctic and eleven stations in the Antarctic (Burns *et al* 2007, 2008).

Input B: Polar cap ionospheric potential

B1: Mansurov effect. Correlation of surface pressure with the superimposed changes in ionospheric potential in the magnetic polar caps due to the solar wind electric field. Persistence \sim 10 days and amplitude 1–2 hPa (Mansurov *et al* 1974, Burns *et al* 2007, 2008).

Input C: Relativistic electron flux

C1: Wilcox effect. First observed as a reduction in the areas of high vorticity in winter storms at times of solar wind HCS crossings. Shown to be more directly correlated with reductions in relativistic electron flux that reduce J_z in years of high stratospheric aerosol loading (Wilcox *et al* 1973, Hines and Halevy 1977, Larsen and Kelly 1977, Tinsley *et al* 1994, Kirkland *et al* 1996).

C2: Kniveton effect. Changes in satellite measured cloud cover (all seasons, global) correlated with reductions in relativistic electron flux for the Pinatubo stratospheric volcanic aerosol era (Kniveton and Tinsley 2004).

C3: Roldugin effect. Reductions in atmospheric transparency (all seasons, mid-high latitudes) correlated with reductions in relativistic electron flux for the El Chicon stratospheric volcanic aerosol era (Roldugin and Tinsley 2004).

C4: Misumi effect. Reductions in 500 hPa temperature of 2–3 K (winters in mid-high northern latitudes) associated with HCS crossings for the Agung stratospheric volcanic aerosol era (Misumi 1983).

Input D: Solar proton events

D1: Schuurmans effect. Pressure increases at 500 hPa pressure altitude centered on the north magnetic pole immediately following solar proton precipitation that increases J_z there.

D2: Veretenenko effect. Increases in areas of high vorticity in winter storms at times and locations of solar proton precipitation. This is in contrast to vorticity area and J_z decreases with relativistic electron flux reductions.

Input E: Cosmic ray Forbush decreases

E1: Roberts effect. First observed as correlations of surface pressure changes in winter storms with the occurrence of magnetic storms. Expressed as changes in the areas of high vorticity in winter storms, the vorticity reductions were found to be more directly correlated with short term (Forbush) decreases in the GCR flux and J_z that accompany most geomagnetic storms (Roberts and Olsen 1973, Padgoankar and Arora 1981, Tinsley *et al* 1989, Tinsley and Deen 1991).

E2: Pudovkin effect. Reductions in high latitude cloud cover correlated with Forbush decreases of GCR, observed from ground stations in Russia (Pudovkin and Veretenenko 1995) and found in global satellite cloud cover data (Todd and Kniveton 2001).

E3: Egorova effect. Changes in atmospheric temperature and pressure above Vostok station, near the south magnetic pole, at times of Forbush decreases of GCR (Egorova *et al* 2000).

Appendix B. List of acronyms

CCN:	cloud condensation nuclei
GADS:	global atmospheric data set
GCR:	galactic cosmic ray
HCS:	heliospheric current sheet
IFN:	ice forming nuclei
IMF:	interplanetary magnetic field
Kp:	planetary index of magnetic activity
PG:	vertical potential gradient
SEP:	solar energetic particle
SG:	specific gravity
STP:	standard temperature and pressure
UV:	ultraviolet

References

- Adlerman E J and Williams E R 1996 Seasonal variations of the global electric circuit *J. Geophys. Res.* **102** 29679–88
- Anderson P C 2004 Subauroral electric fields and magnetospheric convection during the April, 2002 geomagnetic storms *Geophys. Res. Lett.* **31** L11801
- Arijs E, Nevajans D, Ingels J and Frederik P 1983 Positive ion composition measurements between 33 and 20 km altitude *Ann. Geophys.* **1** 161–6
- Bates D R 1982 Recombination of small ions in the troposphere and lower stratosphere *Planet. Space Sci.* **30** 1275–82
- Bauer L A 1925 Correlations between solar activity and atmospheric electricity *Terr. Magn. Atmos. Elect.* **30** 17–22
- Beard K V 1992 Ice initiation in warm-base convective clouds: an assessment of microphysical mechanisms *Atmos. Res.* **28** 125–52
- Beard K V, Ochs H T III and Twohy C H 2004 Aircraft measurements of high average charges on cloud drops in layer clouds *Geophys. Res. Lett.* **31** L14111
- Beer J 2000 Long-term indirect indices of solar variability *Space Sci. Rev.* **94** 53–66
- Benestad R E 2002 *Solar Activity and Earth's Climate* (Berlin: Springer)
- Bering E A III, Few A A and Benbrook J R 1998 The global electric circuit *Phys. Today* **51** 24–30
- Bingen C, Fussen D and Vanhellefont F 2004 A global climatology of stratospheric aerosol size distribution parameters derived from SAGE II data over the period 1984–2000: methodology and climatological observations *J. Geophys. Res.* **109** D06201
- Blanc M and Richmond A D 1980 The ionospheric disturbance dynamo *J. Geophys. Res.* **85** 1669–86
- Bond G, Kromer B, Beer J, Muscheler R, Evans M N, Showers W, Hoffman S, Lotti-Bond R, Haggas I and Bonani G 2001 Persistent solar influence on North Atlantic climate during the Holocene *Science* **294** 2130–6
- Boyle C B, Reiff P H and Hairston M R 1997 Empirical polar cap potentials *J. Geophys. Res.* **102** 111–25
- Bricard J 1965 Action of radioactivity and pollution upon parameters of atmospheric electricity *Problems of Atmospheric and Space Electricity* ed C C Coronity (Amsterdam: Elsevier) pp 82–117
- Brown G M and John J I 1979 Solar cycle influences in tropospheric circulation *J. Atmos. Terr. Phys.* **41** 43–52
- Burns G B, Hesse M H, Parcell S K, Malachowski S and Cole K D 1995 The geoelectric field at Davis Station, Antarctica *J. Atmos. Terr. Phys.* **57** 1783–97
- Burns G B, Frank-Kamenetsky A V, Troshichev O A, Bering E A and Reddell B D 2005 Interannual consistency of bi-monthly differences in diurnal variations of the ground-level, vertical electric field *J. Geophys. Res.* **110** D10106
- Burns G B, Tinsley B A, Klekocuk A R, Troshichev O A, Frank-Kamenetsky A V, Duldig M L, Bering E A and Clem J M 2006 Antarctic polar plateau vertical electric field variations across heliocentric current sheet crossings *J. Atmos. Sol.-Terr. Phys.* **68** 639–54
- Burns G B, Tinsley B A, Frank-Kamenetsky A V and Bering E A 2007 Interplanetary magnetic field and atmospheric electric circuit influences on ground-level pressure at Vostok *J. Geophys. Res.* **112** D04103
- Burns G B, Tinsley B A, French W J R, Troshichev O A and Frank-Kamenetsky A V 2008 Atmospheric circuit influences on ground-level pressure in the Antarctic and Arctic *J. Geophys. Res.* at press
- Byrne G J, Benbrook J R, Bering E A, Oró D, Seubert C O and Sheldon W R 1988 Observations of the stratospheric conductivity and its variations at three latitudes *J. Geophys. Res.* **93** 3879–91
- Chalmers J A 1949/1967 *Atmospheric Electricity* 1st edn (Oxford: Clarendon)
- Chalmers J A 1949/1967 *Atmospheric Electricity* 2nd edn (Oxford: Pergamon)
- Chang E K M and Fu Y 2002 Interdecadal variations in northern hemisphere winter storm track intensity *J. Clim.* **15** 642–58
- Chang E K M, Lee S and Swanson K L 2002 Storm track dynamics *J. Clim.* **15** 2163–83
- Chapman S and Cowling T G 1970 *The Mathematical Theory of Non-Uniform Gases* 3rd edn (London: Cambridge University Press)
- Cobb W E 1967 Evidence of a solar influence on the atmospheric electric elements at Mauna Loa *Mon. Weather Rev.* **95** 905–11
- Curtius J *et al* 2005 Observations of meteoric material and implications for aerosol nucleation in the winter Arctic lower stratosphere derived from in situ particle measurements *Atmos. Chem. Phys.* **5** 3053–69
- Davis M H 1964a Two charged spherical conductors in a uniform electric field: forces and field strength *Q. J. Mech. Appl. Math.* **17** 499–511
- Davis M H 1964b Two charged spherical conductors in a uniform electric field: forces and field strength *Memorandum RM-3860-PR* The RAND Corporation, Santa Monica, CA
- Davis M H 1969 Electrostatic field and force on a dielectric sphere near a conducting plane—a note on the application of electrostatic theory to water droplets *Am. J. Phys.* **37** 26–9
- Davydenko S S, Mareev E A, Marshall T C and Stolzenburg M 2004 On the calculation of electric fields and currents of mesoscale convective systems *J. Geophys. Res.* **109** D111103
- Dentener F, Feichter J and Jueken A 1999 Simulation of the transport of ²²²Rn using on-line and off-line global models at different horizontal resolutions: a detailed comparison with measurements *Tellus Ser. B* **51** 573–602
- Deshler T, Johnson B J and Rozier W R 1993 Balloon-borne measurements of Pinatubo aerosol during 1991 and 1992 at 41°N: vertical profiles, size distribution and volatility *Geophys. Res. Lett.* **20** 1435–8
- Dickinson R E 1975 Solar variability and the lower atmosphere *Bull. Am. Meteorol. Soc.* **56** 1240–8
- Duell B and Duell G 1948 The behavior of barometric pressure during and after solar particle invasions and solar ultraviolet invasions *Smithsonian Miscellaneous Collections* vol 110 (Washington, DC: Smithsonian Institution)
- Eddy J A 1977 Climate and the changing sun *Clim. Change* **1** 173–90
- Eisele F L *et al* 2006 Negative atmospheric ions and their potential role in ion-induced nucleation *J. Geophys. Res.* **111** D04305
- Egorova L V, Vovk V Ya and Troshichev O A 2000 Influence of variations of the cosmic rays on atmospheric pressure and temperature in the Southern geomagnetic pole region *J. Atmos. Sol.-Terr. Phys.* **62** 955–66

- Ermakov H J, Bazilevskaya G A, Pokrevsky P E and Stozhkov Y I 1997 Ion balance equation in the atmosphere *J. Geophys. Res.* **102** 23413–9
- Fischer H-J and Mühleisen R 1972 Variationen des ionosphärenpotentials und der weltgerittertätigkeit im 11-jährigen solaren zyklus *Meteorol. Rundsch.* **25** 6–10
- Fischer H-J and Mühleisen R 1980 The ionospheric potential and the solar magnetic sector boundary crossings *Report Astronomical Institute D-7980*, University of Tübingen, Ravensburg, Germany
- Frahm R A, Winningham J D, Sharber J R, Link R, Crowley G, Gaines E E, Chenette D L, Anderson B J and Potemera T A 1997 The diffuse aurora: a significant source of ionization in the middle atmosphere *J. Geophys. Res.* **102** 28203–14
- Flückiger E, Smart D F and Shea M A 1986 A procedure for estimating the changes in cosmic ray cutoff rigidities and asymptotic directions at low and middle latitudes during periods of enhanced geomagnetic activity *J. Geophys. Res.* **91** 7925–30
- Franklin B 1752 A letter from Mr. Franklin to Mr. Peter Collison, F.R.S. concerning the effects of lightning *Phil. Trans. R. Soc.* **47** 289–91
- Fuchs N A 1934 Über die Stabilität und Aufladung der aerosole *Z. Phys.* **89** 736–43
- Fujioka N, Tsunoda Y, Sugimura A and Arai K 1983 Influence of humidity on ion mobility with lifetime in atmospheric air *IEEE Trans. Power Appar. Syst.* **102** 911–7
- GADS 1998 Global Aerosol Data Set available in 2006 at the URL <http://www.lrz-muenchen.de/~uh234an/www/radaer/gads.html>
- Griffiths R F, Latham J and Myers V 1974 The ionic conductivity of electrified clouds *Q. J. R. Meteorol. Soc.* **100** 181–90
- Gringel W, Rosen J M and Hoffman D J 1986 Electrical structure from 0 to 30 km *The Earth's Electrical Environment* (Washington, DC: National Academy Press) pp 116–82
- Grover S N and Beard K V 1975 A numerical determination of the efficiency with which electrically charged cloud drops and small raindrops collide with electrically charged spherical particles at various densities *J. Atmos. Sci.* **32** 2156–65
- Grover S N, Pruppacher H R and Hamielec A E 1977 A numerical determination of the efficiency with which spherical aerosol particles collide with spherical water drops due to inertial impaction and phoretic and electrical forces *J. Atmos. Sci.* **34** 1655–63
- Gunn R 1954 Diffusion charging of atmospheric droplets by ions and the resulting combination coefficients *J. Meteorol.* **11** 339–47
- Gunn R 1956 The hyperelectrification of raindrops by atmospheric electric fields *J. Meteorol.* **13** 283–8
- Hairston M R and Heelis R A 1990 Model of the high latitude ionospheric convection pattern during southward interplanetary magnetic field, using DE2 data *J. Geophys. Res.* **95** 2333–43
- Hall W D and Beard K V 1975 Electrostatic force between a conducting sphere and a dielectric sphere *Pure Appl. Geophys.* **113** 515–24
- Harrison R G 2004a The global atmospheric circuit and climate *Surv. Geophys.* **25** 441–84
- Harrison R G 2004b Long term correlations in measurements of the global atmospheric electric circuit *J. Atmos. Sol.-Terr. Phys.* **66** 1127–33
- Harrison R G and Carslaw K S 2003 Ion-aerosol-cloud processes in the lower atmosphere *Rev. Geophys.* **41** 1012
- Harrison R G and Stephenson D B 2006 Empirical evidence for a non-linear effect of galactic cosmic rays on clouds *Proc. R. Soc. A* **462** 1221–3
- Hays P B and Roble R G 1979 A quasi-static model of global atmospheric electricity: I. The lower atmosphere *J. Geophys. Res.* **84** 3291–305
- Heaps M G 1978 Parameterization of the cosmic ray ion-production rate above 18 km *Planet. Space Sci.* **26** 513–7
- Herman J R and Goldberg R A 1978 *Sun, Weather and Climate* (Washington, DC: NASA SP-426)
- Hess M, Koepke P and Schult I 1998 Optical properties of aerosols and clouds: the software package OPAC *Bull. Am. Meteorol. Soc.* **79** 831–44
- Hines C O and Halevy I 1977 On the reality and nature of a certain sun-weather correlation *J. Atmos. Sci.* **34** 382–404
- Hobbs P V and Rangno A L 1985 Ice particle concentrations in clouds *J. Atmos. Sci.* **42** 2523–49
- Holzworth R H and Mozer F S 1979 Direct evidence of solar flare modification of atmospheric electric fields *J. Geophys. Res.* **84** 363–7
- Holzworth R H, Norville K W and Williamson P R 1987 Solar flare perturbations in stratospheric current systems *Geophys. Res. Lett.* **14** 852–5
- Hong Y T, Jiang H B, Liu T S, Zhou L P, Beer J, Li H D, Leng X T, Hong B and Qin X G 2000 Response of climate to solar forcing recorded in a 6000-year $\delta^{18}\text{O}$ time-series of Chinese peat cellulose *Holocene* **10** 1–7
- Hoppel W A and Frick G F 1986 Ion-aerosol attachment coefficients and the steady-state charge distribution on aerosols in a bipolar ion environment *Aerosol Sci. Technol.* **5** 1–21
- Hoppel W A, Anderson R V and Willett J C 1986 Atmospheric electricity in the planetary boundary layer *The Earth's Electrical Environment* (Washington, DC: National Academy Press) pp 149–65
- Hoyt D V and Schatten K H 1997 *The Role of the Sun in Climate Change* (New York: Oxford University Press)
- Hu H and Holzworth R H 1996 Observations and parameterization of the stratospheric electrical conductivity *J. Geophys. Res.* **101** 29535–52
- Huth R, Bochníček J and Hejda P 2007 The 11-year solar cycle affects the intensity and annularity of the Arctic Oscillation *J. Atmos. Sol.-Terr. Phys.* **69** 1095–109
- Israël H 1957/1970 *Atmospheric Electricity Vol I, Fundamentals, Conductivity, Ions* 1st edn (Leipzig: Akademische Verlagsgesellschaft) (in German)
- Israël H 1957/1970 *Atmospheric Electricity Vol I, Fundamentals, Conductivity, Ions* 2nd revised edn (Jerusalem: Israel Program for Scientific Translations) 317pp (Engl. Transl.)
- Israël H 1961/1973 *Atmospheric Electricity vol II, Fields, Charges, Currents* 1st edn (Leipzig: Akademische Verlagsgesellschaft) (in German)
- Israël H 1961/1973 *Atmospheric Electricity vol II, Fields, Charges, Currents* 2nd revised edn (Jerusalem: Israel Program for Scientific Translations) 500pp (Engl. Transl.)
- Jones C D and Macpherson B 1997 A latent heat nudging scheme for the assimilation of precipitation data into an operational mesoscale model *Meteorol. Appl.* **4** 269–77
- Kazil J and Lovejoy E R 2004 Tropospheric ionization and aerosol production: a model study *J. Geophys. Res.* **109** D19206
- Keefe D, Nolan P J and Scott J A 1968 Influence of Coulomb and image forces on combination in aerosols *Proc. R. Ir. Acad. A* **66** 17–24
- Kirkland M W, Tinsley B A and Hoeksema J T 1996 Are stratospheric aerosols the missing link between tropospheric vorticity and Earth transits of the heliospheric current sheet? *J. Geophys. Res.* **101** 29689–99
- Klett J D 1972 Charge screening layers around electrified clouds *J. Geophys. Res.* **77** 3187–95
- Kniveton D R and Tinsley B A 2004 Daily changes in global cloud cover and Earth transits of the heliospheric current sheet *J. Geophys. Res.* **109** D11201
- Kniveton D R and Todd M C 2001 On the relationship of cosmic ray flux and precipitation *Geophys. Res. Lett.* **28** 1527–30
- Kodera K 2003 Solar influence on the spatial structure of the NAO during the winter 1900–1999 *Geophys. Res. Lett.* **30** 1175

- Kokorowski M *et al* 2006 Rapid fluctuations of stratospheric electric field following a solar energetic particle event *Geophys. Res. Lett.* **33** L20105
- Lapeyre G and Held I M 2004 The role of moisture in the dynamics and energetics of turbulent baroclinic eddies *J. Atmos. Sci.* **61** 1693–710
- Larsen M F and Kelley M C 1977 A study of an observed and forecasted meteorological index and its relation to the interplanetary magnetic field *Geophys. Res. Lett.* **4** 337–40
- Li X, Temerin M, Baker D N, Reeves G D and Larsen D 2001a Quantitative prediction of radiation belt electrons at geostationary orbit based on solar wind measurements *Geophys. Res. Lett.* **28** 1887–90
- Li X, Baker D N, Kanekal S G, Looper M and Temerin M 2001b Long term measurements of radiation belts by SAMPEX and their variations *Geophys. Res. Lett.* **28** 3827–30
- Lovejoy E R, Curtis J and Froyd K D 2004 Atmospheric ion-induced of sulfuric acid and water *J. Geophys. Res.* **109** D08204
- Lyons W 1996 Sprite observations above the US high plains in relation to their parent thunderstorm systems *J. Geophys. Res.* **101** 29641–52
- Macdonald N J and Roberts W O 1960 Further evidence of a solar corpuscular influence on large-scale circulation at 300 mb *J. Geophys. Res.* **65** 529–34
- MacGorman D R and Rust W D 1998 *The Electrical Nature of Storms* (New York: Oxford University Press) 422pp
- Makino M and Ogawa T 1985 Quantitative estimation of global circuit *J. Geophys. Res.* **90** 5961–6
- Mansurov S M, Mansurova L G, Mansurov G S, Mikhnevich V V, Visotsky A M 1974 North–south asymmetry of geomagnetic and tropospheric events *J. Atmos. Terr. Phys.* **36** 1957–62
- März F 1997 Short term changes in atmospheric electricity associated with Forbush decreases *J. Atmos. Sol.-Terr. Phys.* **59** 975–82
- März F and Harrison R G 2005 Further signatures of long-term changes in atmospheric electrical parameters observed in Europe *Ann. Geophys.* **23** 1987–95
- Markson R 1971 Considerations regarding solar and lunar modulation of geophysical parameters, atmospheric electricity, and thunderstorms *Pure Appl. Geophys.* **84** 161–200
- Markson R 1976 Ionospheric potential variations obtained from aircraft measurements of potential gradient *J. Geophys. Res.* **81** 1980–90
- Markson R 1981 Modulation of the Earth's electric field by cosmic radiation *Nature* **291** 304–8
- Markson R 1985 Aircraft measurements of the atmospheric electrical global circuit during the period 1971–1984 *J. Geophys. Res.* **90** 5967–77
- Markson R 1986 Solar modulation of fair weather and thunderstorm electrification and a proposed program to test an atmospheric electrical sun-weather mechanism *Weather and Climate Responses to Solar Variations* ed B M McCormac (Boulder, CO: Colorado Associated University Press) pp 323–43
- Markson R 2007 The global circuit intensity *Bull. Am. Meteorol. Soc.* **88** 223–41
- Markson R and Muir M 1980 Solar wind control of the Earth's electric field *Science* **208** 979–90
- Marsh N and Svensmark H 2000 Low cloud properties influenced by cosmic rays *Phys. Rev. Lett.* **85** 5004–7
- Martell E A 1985 Enhanced ion production in convective storms by transpired radon isotopes and their decay products *J. Geophys. Res.* **90** 5909–16
- Matsushita S and Maeda H 1965 On the geomagnetic solar quiet day variation field during the IGY *J. Geophys. Res.* **70** 2535–58
- McCracken K G, Beer J and McDonald F B 2004 Variations of cosmic radiation 1890–1986 and the solar and terrestrial implications *Adv. Space Res.* **34** 397–406
- McDaniel E W and Mason E A 1973 *The Mobility and Diffusion of Ions in Gases* (New York: Wiley)
- Meyerott R E, Reagan J B and Evans J E 1986 On the correlation between ionospheric potential and the intensity of cosmic rays *Weather and Climate Responses to Solar Variations* ed B M McCormac (Boulder, CO: Colorado Associated University Press) pp 449–60
- Misumi Y 1983 The tropospheric response to the passage of solar sector boundaries *J. Meteorol. Soc. Japan* **61** 686–94
- Morita Y 1983 Recent measurements of electrical conductivity and ion pair production rate and the ion–ion recombination coefficient derived from them in the lower stratosphere *J. Geomagn. Geoelectr.* **35** 29–38
- Mühlisen R 1971 New determination of the air-earth current over the ocean and measurements of ionospheric potential *Pure Appl. Geophys.* **84** 112–5
- Mühlisen R 1977 The global electric circuit and its parameters *Electrical Processes in Atmospheres* ed H Dolezalek and R Reiter (Darmstadt: Steinkopff) pp 467–76
- NAS 1986 *The Earth's Electrical Environment* (Washington, DC: Geophysics Research Board, US National Academy of Sciences Press)
- Neher H V 1967 Cosmic ray particles that changed from 1954 to 1958 to 1965 *J. Geophys. Res.* **72** 1527–39
- Neher H V 1971 Cosmic rays at high latitudes and altitudes covering four solar maxima *J. Geophys. Res.* **76** 1637–51
- Neff U, Burns S J, Mangini A, Mudelsee M, Fleitmann D and Matter A 2001 Strong coherence between solar variability and the monsoon in Oman between 9 and 6 kyr ago *Nature* **411** 290–3
- Olson R H, Roberts W O and Gerety E 1977 Vorticity area index 1946–1976 *Solar Terrestrial Physics and Meteorology: Working Document—II, Report by World Data Center A, NOAA* ed A H Shapley and H W Kroel (Washington, DC: SCOSTEP, National Academy of Sciences) pp 83–114
- Olson R H, Roberts W O and Gerety E 1979 Vorticity area index 1976–1978 *Solar Terrestrial Physics and Meteorology: Working Document—III, Report by World Data Center A, NOAA* ed A H Shapley *et al* (Washington, DC: SCOSTEP, National Academy of Sciences) pp 86–8
- Olson R H, Roberts W O and Zerefos C S 1975 Short-term relationships between solar flares, geomagnetic storms and tropospheric vorticity patterns *Nature* **257** 113–5
- Olson D E 1983 Interpretation of the solar influence on the atmospheric electrical parameters *Weather and Climate Responses to Solar Variations* ed B M McCormac (Boulder, CO: Colorado Associated University Press) pp 483–8
- Padgoankar A D and Arora B R 1981 Tropospheric vorticity responses to the solar magnetic sector structure and geomagnetic disturbances *Pure Appl. Geophys.* **119** 893–900
- Parish T R and Bromwich D H 1991 Continental scale simulation of the Antarctic katabatic wind regime *J. Clim.* **4** 135–46
- Pasco V P, Inam U S and Bell T F 1998 Ionospheric effects due to electrostatic thunderstorm fields *J. Atmos. Sol.-Terr. Phys.* **60** 863–70
- Posselt D J and Martin J E 2004 The effect of latent heat release on the evolution of a warm occluded thermal structure *Mon. Weather Rev.* **132** 578–99
- Pruppacher H R and Klett J D 1997 *Microphysics of Clouds and Precipitation* 2nd edn (New York: Springer) 954pp
- Pudovkin M I and Veretenenko S V 1995 Cloudiness decreases associated with Forbush-decreases of galactic cosmic rays *J. Atmos. Sol.-Terr. Phys.* **57** 1349–55
- Pumpyan P E, Chernysheva S P, Sheftel V M and Yaroshenko A N 1987 Solar-magnetospheric effects in the variations of the atmospheric electric field in the high latitude zone *Geomagn. Aeron.* **27** 244–7 (Engl. Transl.)
- Rakov V A and Uman M A 2003 *Lightning, Physics and Effects* (Cambridge, UK: Cambridge University Press) 687pp

- Ram M and Stolz M 1999 Possible solar influences on the dust profile of the GISP2 ice core from central Greenland *Geophys. Res. Lett.* **26** 1043–6
- Reiter R 1969 Solar flares and their impact on potential gradient and air-earth current characteristics at high mountain stations *Pure Appl. Geophys.* **72** 259–67
- Reiter R 1977 The electric potential of the ionosphere as controlled by the solar magnetic sector structure. Results from a study over the period of a solar cycle *J. Atmos. Terr. Phys.* **39** 95–9
- Reiter R R 1992 *Phenomena in Atmospheric and Environmental Electricity* (Amsterdam: Elsevier) 541pp
- Richmond A D 1976 Electric fields in the ionosphere and plasmasphere on quiet days *J. Geophys. Res.* **81** 1447–50
- Roberts W O and Olson R H 1973 Geomagnetic storms and wintertime 300 mb trough development in the North Pacific–North America area *J. Atmos. Sci.* **30** 135–40
- Roble R G and Hays P B 1979 A quasi-static model of atmospheric electricity: II. Electrical coupling between the upper and lower atmosphere *J. Geophys. Res.* **84** 7247–56
- Roble R G and Tzur I 1986 The global atmospheric electric circuit, *The Earth's Electrical Environment* (Washington, DC: National Academy Press) pp 201–31
- Rogers R R and Yau M K 1989 *A Short Course in Cloud Physics* 3rd edn (Oxford, UK: Pergamon)
- Roldugin V C and Tinsley B A 2004 Atmospheric transparency changes associated with solar wind-induced atmospheric electricity variations *J. Atmos. Sol.-Terr. Phys.* **66** 1143–9
- Rosen J M and Hoffman D J 1981 Balloon borne measurements of electrical conductivity, mobility and the recombination coefficient *J. Geophys. Res.* **86** 7406–10
- Rosen J M and Hoffman D J 1988 A search for large ions in the stratosphere *J. Geophys. Res.* **93** 8415–22
- Rossow W B and Lacis A A 1990 Global, seasonal cloud variations from satellite radiance measurements: II. Cloud properties and radiative effects *J. Clim.* **3** 1204–53
- Rostoker G and Sharma R P 1980 Correlation of high latitude tropospheric pressure with the structure of the interplanetary magnetic field *Can. J. Phys.* **58** 255–9
- Ruddiman W F 2001 *Earth's Climate Past and Future* (New York: Freeman)
- Rutledge S A and Hobbs P V 1983 The mesoscale and microscale structure and organization of clouds and precipitation in midlatitude cyclones: VIII. A model for the 'Seeder Feeder' process in warm frontal rainbands *J. Atmos. Sci.* **40** 1185–206
- Rycroft M J 2006 Electrical processes coupling the atmosphere and the ionosphere: an overview *J. Atmos. Sol.-Terr. Phys.* **68** 445–56
- Rycroft M J and Cho M 1998 Modeling electric and magnetic fields due to thunderclouds and lightning from cloud tops to the ionosphere *J. Atmos. Sol.-Terr. Phys.* **60** 889–93
- Sapkota B K and Varshneya N C 1990 On the global atmospheric electric circuit *J. Atmos. Sol.-Terr. Phys.* **50** 1–20
- Schlamp R J, Grover S N, Pruppacher H R and Hamielec A E 1976 A numerical investigation of the effect of electric charges and vertical external electric fields on the collision efficiency of cloud drops *J. Atmos. Sci.* **33** 1747–55
- Schlamp R J, Grover S N, Pruppacher H R and Hamielec A E 1979 A numerical investigation of the effect of electric charges and vertical external electric fields on the collision efficiency of cloud drops: II *J. Atmos. Sci.* **362** 339–49
- Schuermans C J E 1965 Influence of solar flare particles on the general circulation of the atmosphere *Nature* **205** 167–8
- Schuermans C J E and Oort A H 1969 A statistical study of pressure changes in the troposphere and lower stratosphere after strong solar flares *Pure Appl. Geophys.* **75** 233–46
- Seibert H, Stratmann F and Wehner B 2004 First observations of increased ultrafine particle number concentrations near the inversion of a continental planetary boundary layer and its relation to ground-based measurements *Geophys. Res. Lett.* **31** L09102
- Sentman D D and Wescott E M 1995 Red sprites and blue jets: thunderstorm-excited optical emissions in the stratosphere, mesosphere and ionosphere *Phys. Plasmas* **2** 2514–22
- Shea M A and Smart D F 2004 Preliminary study of cosmic rays, geomagnetic field changes and possible climate changes *Adv. Space Res.* **34** 420–5
- Siingh D *et al* 2007 The atmospheric global electric circuit: an overview *Atmos. Res.* **84** 91–110
- Smart D F and Shea M A 1985 Galactic cosmic radiation and solar energetic particles *Handbook of Geophysics and the Space Environment* ed A S Jursa (Air Force Geophysics Laboratory, USAF) chapter 6
- Smith D and Adams N G 1982 Ionic recombination in the stratosphere *Geophys. Res. Lett.* **9** 1085–7
- Snetsinger K G, Ferry G V, Russell P B, Pueschel R F, Oberbeck V R, Hays D M and Fong W 1987 Effects of El Chichon on stratospheric aerosols late 1982 to early 1984 *J. Geophys. Res.* **92** 14761–71
- Soula S, Chauzy S, Chong M, Coquillat S, Georgis J F, Seity Y and Tabary P 2003 Surface precipitation electric current produced by convective rains during the Mesoscale Alpine Program *J. Geophys. Res.* **108** 4395
- Stephens G L *et al* 2002 The Cloudsat mission and the A-train *Bull. Am. Meteorol. Soc.* **83** 1771–90
- Stolzenburg M, Marshall T C, Rust W D and Bartels D L 2002 Two simultaneous charge structures in thunderstorm convection *J. Geophys. Res.* **107** 4352
- Stow C D 1969 Atmospheric electricity *Rep. Prog. Phys.* **32** 1–67
- Stuiver M, Grootes P M and Braziunas T 1995 The GISP2 $\Delta^{18}\text{O}$ climate record of the past 16 000 years and the role of the sun, ocean and volcanoes *Quaternary Res.* **44** 341–54
- Svensmark H and Friis-Christensen E 1997 Variation of cosmic ray flux and global cloud coverage: a missing link in sun-climate relationships *J. Atmos. Sol.-Terr. Phys.* **59** 1225–32
- Svensmark H, Pedersen J O, Marsh N D, Enghoff M B and Uggerhøj U I 2007 Experimental evidence for the role of ions in particle nucleation under atmospheric conditions *Proc. R. Soc. A* **463** 385–96
- Takahashi T 1973 Measurements of electric charges on cloud droplets, drizzle and raindrops *Rev. Geophys. Space Phys.* **11** 903–24
- Takemura T, Kaufman Y J, Remer L A and Nakajima T 2007 Two competing pathways of aerosol effects on cloud and precipitation formation *Geophys. Res. Lett.* **34** L04802
- Thejll P 2002 Calculation of relative vorticity and the vorticity area index from NCEP reanalysis data *Danish Meteorological Institute Technical Report* 02-26
- Tinsley B A and Deen G W 1991 Apparent tropospheric response to MeV–GeV particle flux variations, a connection via electrofreezing of supercooled water in high level clouds? *J. Geophys. Res.* **96** 2283–96
- Tinsley B A and Heelis R A 1993 Correlations of atmospheric dynamics with solar activity; evidence for a connection via the solar wind, atmospheric electricity, and cloud microphysics *J. Geophys. Res.* **98** 10375–84
- Tinsley B A and Zhou L 2006 Initial results of a global circuit model with stratospheric and tropospheric aerosols *J. Geophys. Res.* **111** D16205
- Tinsley B A, Brown G M and Scherrer P H 1989 Solar variability influences on weather and climate: possible connections through cosmic ray fluxes and storm intensification *J. Geophys. Res.* **94** 14783–92
- Tinsley B A, Hoeksema J T and Baker D N 1994 Stratospheric volcanic aerosols and changes in air-earth current density at solar wind magnetic sector boundaries as conditions for the Wilcox tropospheric vorticity effect *J. Geophys. Res.* **99** 16805–13

- Tinsley B A, Liu W, Rohrbaugh R P and Kirkland M W 1998 South Pole electric field responses to overhead ionospheric convection *J. Geophys. Res.* **103** 26137–46
- Tinsley B A, Rohrbaugh R P, Hei M and Beard K V 2000 Effects of image charges on the scavenging of aerosol particles by cloud droplets and on droplet charging and possible ice nucleation processes *J. Atmos. Sci.* **57** 2118–34
- Tinsley B A, Burns G B and Hei M 2001 Electroscavenging in clouds with broad droplet size distributions and weak electrification *Atmos. Res.* **59–60** 115–36
- Tinsley B A, Zhou L and Plemmons A 2006 Changes in scavenging of particles by droplets due to weak electrification in clouds *Atmos. Res.* **79** 266–95
- Tinsley B A, Burns G B and Zhou L 2007 The role of the global electric circuit in solar and internal forcing of clouds and climate *Adv. Space Res.* **40** 1126–39
- Todd M C and Kniveton D R 2001 Changes in cloud cover associated with Forbush decreases of galactic cosmic rays *J. Geophys. Res.* **106** 32031–42
- Torreson O W, Gish O H, Parkinson W C and Wait G R 1946 *Scientific Results of Cruise VII of the Carnegie during 1928–29* (Washington, DC: Carnegie Institution) Publication No 568
- Tripathi S N and Harrison R G 2002 Enhancement of contact nucleation by scavenging of charged aerosol *Atmos. Res.* **62** 57–70
- Tripathi S N, Vishnoi S, Kumar S and Harrison R G 2006 Computationally-efficient expressions for the collision efficiency between electrically charged aerosol particles and cloud droplets *Q. J. R. Meteorol. Soc.* **132** 1717–31
- Troshichev O A and Janzhura A 2004 Temperature alterations on the Antarctic ice sheet initiated by the disturbed solar wind *J. Atmos. Sol.-Terr. Phys.* **66** 1159–72
- Tzur I, Roble R G, Zhuang H C and Reid G C 1983 The response of the Earth's global electric circuit to a solar proton event *Weather and Climate Responses to Solar Variations* ed B M McCormac (Boulder, USA: Colorado Associated University Press) pp 427–35
- Uldehufen P M and Cess R P 2001 cloud cover variations over the United States: an influence of cosmic rays or solar variability *Geophys. Res. Lett.* **28** 2617–20
- Usoskin I G, Voiculescu M, Kovalstov G A and Mursula K 2006 Correlation of clouds at different altitudes and solar activity: fact or artifact? *J. Atmos. Sol.-Terr. Phys.* **68** 2164–72
- van Loon H and Labitzke K 1988 Association between the 11 year solar cycle, the QBO and the atmosphere: III. Surface and 700 mb on the northern hemisphere in winter *J. Clim.* **1** 905–20
- van Loon H and Shea D J 1999 A probable signal of the 11-year solar cycle in the troposphere in the northern hemisphere *Geophys. Res. Lett.* **26** 2893–6
- Venne D E and Dartt D G 1990 An examination of possible solar cycle-QBO effects in the northern hemisphere troposphere *J. Clim.* **3** 272–81
- Veretenenko S V and Pudovkin M I 1997 Effects of Galactic cosmic ray variations on the solar radiation input in the lower atmosphere *J. Atmos. Terr. Phys.* **59** 1739–46
- Veretenenko S V and Pudovkin M I 1999 Variations of solar radiation input into the lower atmosphere associated with different helio/geophysical factors *J. Atmos. Sol.-Terr. Phys.* **61** 521–9
- Veretenenko S V and Pudovkin M I 2000 Latitudinal dependence of helio/geophysical effects on the solar radiation input to the lower atmosphere *J. Atmos. Sol.-Terr. Phys.* **62** 567–71
- Veretenenko S and Thejll P 2004 Effects of energetic solar protons events on the cyclone development in the North Atlantic *J. Atmos. Sol.-Terr. Phys.* **66** 393–405
- Veretenenko S and Thejll P 2005 Cyclone regeneration in the North Atlantic intensified by energetic solar proton events *Adv. Space Res.* **35** 470–5
- Wang Y, Cheng H, Edwards R L, He Y, Kong X, An Z, Wu J, Kelly M J, Dykoski C A and Li X 2005 The Holocene Asian monsoon: links to solar changes and North Atlantic climate *Science* **308** 854–7
- Weimer D R 1996 A flexible, IMF dependent model of high latitude electric potentials having 'space weather' applications *Geophys. Res. Lett.* **23** 2549–52
- Weimer D R 2001 An improved model of ionospheric electric potentials including substorm perturbations and application to the Geospace Environment Modeling November 24, 1996, event *J. Geophys. Res.* **106** 407–16
- Whipple F J W 1929 On the association of the diurnal variation of electric potential on fine weather with the distribution of thunderstorms over the globe *Q. J. R. Meteorol. Soc.* **55** 1–17
- Wilcox J M, Scherrer P H, Svalgaard L, Roberts W O and Olson R H 1973 Solar magnetic structure: relation to circulation of the Earth's atmosphere *Science* **180** 185–6
- Williams E R 2005 Lightning and climate: a review *Atmos. Res.* **76** 272–87
- Williams R G and Gerety E J 1978 Does the troposphere respond to day-to-day changes in solar magnetic field? *Nature* **275** 200–1
- Wilson C T R 1920 Investigations on lightning discharges and on the electric field and thunderstorms *Phil. Trans. R. Soc. Lond.* **A 221** 73–115
- Yair Y and Levin Z 1989 Charging of polydisperse aerosol particles by attachment of atmospheric ions *J. Geophys. Res.* **94** 13085–901
- Young K C 1993 *Microphysical Processes in Clouds* (Oxford, UK: Oxford University Press)
- Yu F 2002 Altitude variations of cosmic ray induced production of aerosols: implications for global cloudiness and climate *J. Geophys. Res.* **107** 1118
- Yu F and Turco R P 2001 From molecular clusters to nanoparticles: role of ambient ionization in tropospheric aerosol formation *J. Geophys. Res.* **106** 4797–814
- Zhao X and Hundhausen A J 1983 Spatial structure of the solar wind in 1976 *J. Geophys. Res.* **88** 451–4
- Zhou L and Tinsley B A 2007 The production of space charge at the boundaries of layer clouds *J. Geophys. Res.* **112** D11203